NASA TM SX-296

Declassified by authority of NASA
Classification Change Notices No. 113
Dated ** 6-28-67

IN-08
380 443

TECHNICAL MEMORANDUM

SX-296

for the

U. S. Air Force

PERFORMANCE, STABILITY, AND CONTROL INVESTIGATION

AT MACH NUMBERS FROM 0.4 TO 0.9 OF A MODEL OF

THE "SWALLOW" WITH OUTER WING PANELS

SWEPT 25° WITH AND WITHOUT

POWER SIMULATION

By Jack F. Runckel, James W. Schmeer,
and Marlowe D. Cassetti

Langley Research Center
Langley Field, Va.

NATIONAL AERONAUTICS AND SPACE ADMINISTRATION

WASHINGTON

MAY 3 1960

NATIONAL AERONAUTICS AND SPACE ADMINISTRATION

TECHNICAL MEMORANDUM SX-296

for the

U.S. Air Force

PERFORMANCE, STABILITY, AND CONTROL INVESTIGATION

AT MACH NUMBERS FROM 0.4 TO 0.9 OF A MODEL OF

THE "SWALLOW" WITH OUTER WING PANELS

SWEPT 25° WITH AND WITHOUT

POWER SIMULATION*

By Jack F. Runckel, James W. Schmeer,
and Marlowe D. Cassetti

SUMMARY

An investigation of the performance, stability, and control characteristics of a variable-sweep arrow-wing model (the "Swallow") with the outer wing panels swept 25° has been conducted in the Langley 16-foot transonic tunnel. The wing was uncambered and untwisted and had RAE 102 airfoil sections with a thickness-to-chord ratio of 0.14 normal to the leading edge. Four outboard engines located above and below the wing provided propulsive thrust, and, by deflecting in the pitch direction and rotating in the lateral plane, also produced control forces. A pair of swept lateral fins and a single vertical fin were mounted on each engine nacelle to provide aerodynamic stability and control. Jets-off data were obtained with flow-through nacelles, simulating the effects of inlet flow; jet thrust and hot-jet interference effects were obtained with faired-nose nacelles housing hydrogen peroxide gas generators.

Six-component force and moment data were obtained through a Mach number range of 0.40 to 0.90 at angles of attack and angles of sideslip from 0° to 15°. Longitudinal, directional, and lateral control were obtained by deflecting the nacelle-fin combinations as elevators, rudders, and ailerons at several fixed angles for each control. Jet effects were

*Title, Confidential.

L-975

obtained at jet total-pressure ratios from 1.0 to 4.0. In addition, the effects on longitudinal and directional stability of power loss in one engine were investigated.

The results indicate that the basic wing-body became unstable at low lift coefficients and the addition of nacelles with fins delayed instability to only a slightly higher lift coefficient. Two nacelles mounted on the upper wing surface caused larger losses in lift-drag ratio than two mounted under the wing and toeing-in four nacelles greatly reduced maximum lift-drag ratios as compared with four nacelles alined with the free stream. The nacelle-fin combinations were ineffective as longitudinal controls but were adequate for providing directional and lateral control. The model with nacelles and fins was directionally stable at all test conditions and the directional stability was about the same as that for a similar model having a cambered wing. Jet interference effects on stability and control characteristics were small but the effects on drag were appreciable; the drag effects were favorable at some test conditions. Loss of power on one engine had little effect on longitudinal stability; the effects on directional stability although larger were controllable with small nacelle deflections.

INTRODUCTION

The concept of a variable-sweep-wing aircraft has been considered as a means of achieving efficient take-off and low-speed performance combined with supersonic flight capabilities. An example of this type of configuration was the Bell X-5 research airplane in which the wing could be swept and translated while in flight (ref. 1).

Vickers-Armstrongs (Aircraft), Ltd., has recently proposed a variable-sweep arrangement having an arrow wing which has been designated the Swallow. The Swallow is essentially an all-wing airplane on which the outer wing panels can be varied from a leading-edge sweep of 20° to 80° while in flight. The advantages claimed for this design (ref. 2) are (1) increased efficiency by eliminating all nonlifting surfaces including the fuselage and empennage, (2) good take-off and landing characteristics due to the low wing loading, (3) good low-speed characteristics with the high-aspect-ratio wing at low sweep angles, (4) the ability to adjust the sweep to obtain the best lift-drag ratio at each Mach number, and (5) good high-speed flight characteristics are achieved with high sweep, low aspect ratio, and effectively thinner wings. The development of a suitable wing pivot and sweep mechanism had been achieved by Vickers-Armstrongs (Aircraft), Ltd., and a proposal for a 50,000-pound "strike" aircraft version of the Swallow was presented in reference 3.

Control of the airplane was originally intended to be obtained by deflecting outboard turbojet engine nacelles located above and below the wings in the pitch direction and by rotating them in a lateral plane. However, low-speed wind-tunnel tests indicated that sufficient control would not be available by deflecting the nacelles alone; therefore, swept fin surfaces were added to the upper, lower, and side surfaces of the nacelles as indicated in reference 4. In addition, it was found that with the wings swept 25° the directional stability was increased when the nacelles were toed-in 10° from the streamwise direction.

Because of the unique arrangement of the engines, which provide both propulsive thrust and a portion of the control from components of the jet vectors, an investigation was conducted in the Langley 16-foot transonic tunnel to determine the performance, stability, and control characteristics of a 1/12-scale model of the Swallow with and without jet simulation. Two nacelle configurations were tested: airflow nacelles which simulated the engine inlet flow, and jet nacelles with faired inlets which simulated the jet thrust characteristics. The effectiveness of the nacelle-fin combination as aerodynamic controls without engine power was obtained from tests on the airflow-nacelle configuration; the jet interference effects on stability and control were determined from the jets-on tests. In addition, stability information has been obtained for the one-engine-out condition during the power-on part of the investigation. The model wing was the same as the Swallow wing in plan form and thickness distribution but was uncambered and the model fuselage volume was somewhat less than that proposed by Vickers-Armstrongs (ref. 3). The results reported herein were obtained on a model with an outboard-wing sweep angle of 25°, corresponding to a subsonic-flight configuration of the Swallow aircraft.

Tests were conducted at Mach numbers of 0.4, 0.6, 0.8, and 0.9, at angles of attack from 0° to 14°, and at sideslip angles from 0° to 15°. For the jets-on portion of the investigation, jet pressure ratios of 1 (jets off), 2, 3, and 4 were utilized. Finned-nacelle deflections from 0° to ±15° and 0° to -30° differential deflection in the pitch plane and ±10° from an initial toe-in angle of 10° in the lateral plane were set to correspond to airplane elevator, aileron, and rudder deflections, respectively. Reynolds number per foot varied from about 2.5×10^6 at low Mach numbers to approximately 4×10^6 at the highest test Mach number.

COEFFICIENTS AND SYMBOLS

All coefficients except lift and drag are presented for the body axes system. The wing area includes the area of both the forewing and the outer panels. Moments have been taken about a point located at the trailing-edge apex for a wing sweep angle of 80°.

SECRET

Coefficients

Model with airflow nacelles:

C_D drag coefficient, $\dfrac{\text{Drag}}{qS}$

$C_{D,i}$ nacelle internal drag coefficient, $\dfrac{\text{Internal drag}}{qS}$

$C_{D,o}$ minimum drag coefficient

C_L lift coefficient, $\dfrac{\text{Lift}}{qS}$

C_l rolling-moment coefficient, $\dfrac{\text{Rolling moment}}{qSb}$

C_m pitching-moment coefficient, $\dfrac{\text{Pitching moment}}{qSc_r}$

C_n yawing-moment coefficient, $\dfrac{\text{Yawing moment}}{qSb}$

$C_{p,b}$ base pressure coefficient, $\dfrac{p_b - p}{q}$

C_Y side-force coefficient, $\dfrac{\text{Side force}}{qS}$

Model with jet nacelles:

$C_{D,t}$ total drag coefficient

$C_{L,t}$ total lift coefficient

$C_{l,t}$ total rolling-moment coefficient

$C_{m,t}$ total pitching-moment coefficient

$C_{n,t}$ total yawing-moment coefficient

$C_{Y,t}$ total side-force coefficient

} Model coefficients including components of jet thrust

$C_{D,j}$ drag coefficient

$C_{L,j}$ lift coefficient

$C_{l,j}$ rolling-moment coefficient

$C_{m,j}$ pitching-moment coefficient

$C_{n,j}$ yawing-moment coefficient

$C_{Y,j}$ side-force coefficient

} Model coefficients with applicable components of jet thrust removed

$\Delta C_{D,j}$ interference drag coefficient, $\left(C_{D,j}\right)_{\text{jets on}} - \left(C_{D,j}\right)_{\text{jets off}}$

C_F jet thrust coefficient, $\dfrac{F_j}{pA_j}$

Symbols

A cross-sectional area, sq ft

A_j jet-nacelle exit area, sq ft

b wing span, ft

c chord

c_r root chord ($\Lambda = 80^\circ$), ft

F_j jet thrust, lb

l maximum model length, axial distance from nose to nacelle exit, 71.3 in.

M free-stream Mach number

p free-stream static pressure, lb/sq ft

p_b base pressure, lb/sq ft

q   free-stream dynamic pressure, lb/sq ft

r   radius, in.

S   wing area ($\Lambda = 25^\circ$), sq ft

t   thickness

x   axial distance

y   airfoil-thickness ordinate

α angle of attack, deg

β angle of sideslip, deg

δ nacelle lateral deflection, positive nose right, deg

$\Delta\delta$ increment from basic 10° toe-in, deg

θ nacelle pitch deflection, positive nose up, deg

$\Delta\theta$ nacelle differential deflection in pitch plane, deg

Λ leading-edge sweep angle of outboard portion of wing, deg

ϕ meridian angle, deg

Parameters:

C_{L_α} lift-curve slope, per deg

$C_{l_{\Delta\theta}}$ lateral control effectiveness parameter, per deg

$C_{m_{C_L}}$ static longitudinal stability parameter, per deg

C_{m_θ} longitudinal control effectiveness parameter, per deg

$C_{n_{\Delta\delta}}$ directional control effectiveness parameter, per deg

$C_{n_\beta} = \dfrac{\partial C_n}{\partial \beta}$, per deg

L/D   lift-drag ratio

$P_{t,J}/P$ jet total-pressure ratio

Subscripts:

L   left

R   right

max   maximum

1   outer

2   inner

MODEL AND APPARATUS

Tunnel and Model

The investigation reported herein was conducted in the Langley
16-foot transonic tunnel. A 1/12-scale version of a 50,000-pound
Swallow strike aircraft (ref. 3) was tested in the low-sweep configura-
tion corresponding to flight at subsonic speeds. A sketch of the model
with outer wing panels swept 25° is shown in figure 1. The inner wing
panel is fixed at a sweep of 80° for the Swallow design. Wing pivot
points were located at the intersection of 49 percent of the semispan
for $\Lambda = 80^\circ$ and the quarter-chord line. RAE 102 airfoil sections,
14 percent thick normal to the leading edge, were employed in the
uncambered wing (table 1). The body extended downstream to about the
wing-tip trailing-edge station for $\Lambda = 25^\circ$ and was just large enough
to enclose a six-component strain-gage balance which was attached to a
sting support. The wing-body combination was tested without nacelles
and with various nacelle arrangements.

The pivots of the nacelles were located at the 25-percent chord and
78-percent-semispan stations (for $\Lambda = 80^\circ$). Two sets of engine nacelles
each having swept horizontal and vertical finned surfaces were utilized
in the tests. The airflow nacelles, figure 2(a), simulated the turbojet-
engine nacelle inlet which has a central cone. For one configuration
these nacelles were installed one below each semispan (fig. 2(b)) and on
another configuration they were installed one above each semispan. For
all other configurations the model had one nacelle above and one below
each semispan. The nacelle center lines were separated vertically by
two nacelle diameters with a constant-chord pylon and the nacelles could

be deflected in a vertical plane or in a lateral plane as indicated in figure 3. The basic nacelle setting for the model with $\Lambda = 25^\circ$ had no deflection in the vertical plane ($\theta = 0^\circ$) and 10° toe-in ($\delta_L = 10^\circ$, $\delta_R = -10^\circ$) in the lateral plane. Swept fins were added to the nacelles as aerodynamic surfaces for obtaining additional control which had been found to be insufficient with the nacelles alone (ref. 4). Pitch and roll control could be obtained by deflecting the nacelle-fin combinations in the vertical plane and directional control was obtained by rotating them in a lateral plane. On each wing the pylons and nacelles rotated as a unit for directional control.

The jet nacelles had the same external shape as the flow-through nacelles except that a faired nose having the same cone angle as the central spike of the airflow nacelles was attached at the inlet station. In addition, the base area of the jet nacelles was slightly larger than that of the airflow nacelles and a somewhat thicker fairing was used for the pylon to provide room for the propellant line (fig. 3). The exit areas of the jet nacelles were scaled to approximate those proposed for the Bristol turbojet engine (BE-38) but the clamshell exits were replaced with conical exits. Concentrated hydrogen peroxide was conducted through lines in the model and into the nacelles which contained a decomposition chamber similar to that described in reference 5. The monopropellant was decomposed by a catalyst in the chamber to produce an exhaust gas at $1,350^\circ$ F which simulated the hot jet of the Swallow's turbojet engines. Photographs of the model with jet nacelles set at various deflection angles are presented in figure 4.

The Swallow was designed to have a smooth area progression with a basic-wing sweepback of 80°. The area progression for the present model with an outboard wing sweep of 25° alone and with four nacelles added is shown in figure 5.

Model forces and moments were obtained from a six-component internal strain-gage balance. Nacelle annulus and fuselage base pressures were measured on all configurations. Nacelle internal drag was obtained from total- and static-pressure tubes inside the airflow nacelles and jet total pressure was measured in the tailpipe of the jet nacelles as indicated in figure 3. Model angle of attack was obtained from an internal pendulum strain-gage indicator.

TESTS, CORRECTIONS, AND ACCURACY

Tests

All configurations were tested with transition fixed on the wing. The transition consisted of 1/8-inch-wide bands of size 180 carborundum

grain at the $2\frac{1}{2}$- percent-chord station and extended over the full wing span. The grain size was determined by the method discussed in reference 6.

Wing-body configuration alone and with airflow nacelles.- The wing-body combination was tested at Mach numbers of 0.4, 0.6, 0.8, and 0.9 at angles of attack from -2° to about 14°. A short investigation was conducted to determine the effect of nacelle placement and toe-in angle on the aerodynamic characteristics at Mach numbers from 0.4 to 0.9. The basic nacelle toe-in configuration (θ = 0°, δ_L = 10°, and δ_R = -10°) was also tested without transition.

Control effectiveness at zero sideslip was determined at Mach numbers of 0.4, 0.6, and 0.8 at angles of attack from 0° to 12° or 14° for longitudinal control deflections of θ = 0°, 7.5°, -7.5°, and -15° at δ_L = 10 and δ_R = -10° (nacelle-fin combination acting as elevators), and for directional control deflections of $\Delta\delta$ = 0° (δ_L = 10°, δ_R = -10°), $\Delta\delta$ = 5° (δ_L = 15°, δ_R = -5°), $\Delta\delta$ = -5° (δ_L = 5°, δ_R = -15°), and $\Delta\delta$ = -10° (δ_L = 0°, δ_R = -20°) at θ = 0° (pylon-nacelle-fin combination operating as rudders).

The basic toe-in configuration was also tested in sideslip at α = 0° and β = 0°, 5°, 10°, and 15° at Mach numbers of 0.4, 0.6, and 0.8.

Jet nacelles.- Power-off tests were conducted with the jet nacelles deflected differentially as ailerons for lateral control at $\Delta\theta$ = 0°, $\Delta\theta$ = -15° (θ_L = -7.5°, θ_R = 7.5°), $\Delta\theta$ = -30° (θ_L = -15°, θ_R = 15°) with δ_L = 10° and δ_R = -10° at β = 0°, at α from 0° to about 10°, and at Mach numbers of 0.4 and 0.6. Similar differential deflections were investigated with power on at jet total-pressure ratios of approximately 1, 2, 3, and 4 at α = 4° and M = 0.4 and 0.6.

Longitudinal control effectiveness was determined at jet pressure ratios from 1 to about 4 for the same range of θ-deflections and Mach numbers as the airflow nacelles but at angles of attack of 0°, 4°, and 8°. The model was tested over the same power setting range with directional control deflections of $\Delta\delta$ = 0°, 5°, 10°, -5°, and -10° at α = 4° and Mach numbers of 0.4 and 0.6 at both β = 0° and 5°. In addition, the model longitudinal and directional stability and control with one jet engine out was investigated at Mach numbers of 0.4 and 0.6.

Static tests were performed on each engine nacelle to determine the variation of thrust coefficient with jet pressure ratio.

Corrections

Wing-body combination alone and with airflow nacelles.- The data have been adjusted to free-stream static pressure at the fuselage base and have been corrected for the effects of the internal drag where applicable. No corrections were applied for the base drag on the air-flow nacelles since this correction amounted to less than 0.0001 in drag coefficient in all cases. Fuselage base pressure coefficients are presented in figure 6(a), and average internal drag coefficients for the upper and lower nacelles are shown in figure 6(b).

Model with jet nacelles.- All coefficients have been adjusted to the condition of free-stream static pressure at the fuselage base and at the nacelle annular bases for the jets-on case. For the jets-off case, the data were further adjusted to the condition of free-stream static pressure acting on the jet exit areas. Jet-nacelle base pressure coefficients are presented in figure 7(a). Each jet simulator was stat-ically calibrated in a manner similar to that described in reference 5. The static-jet-thrust calibrations for the jet simulators are given in figure 7(b).

Coefficients for the jet-nacelle configurations are presented in three forms. (See section entitled "Symbols.") The coefficients with the subscript t include components of the jet thrust. These coeffi-cients are made up of aerodynamic, jet thrust, and jet interference forces. Coefficients with the subscript j represent data with com-ponents of the jet thrust removed. The jet thrust of each nacelle was determined by using measured jet pressure ratios and the static thrust calibrations. These coefficients are made up of aerodynamic plus jet interference forces. In the cases where jet interference effects are apparent, an incremental coefficient is also used. This is the jet interference coefficient obtained by removal of the jets-off aerodynamic value from the jets-on aerodynamic plus jet interference coefficient.

No corrections for wing aeroelastic effects have been included in the data presented. Rolling-moment data has been corrected for induced effects due to tunnel airflow angularity and model asymmetry by sub-tracting the rolling-moment coefficients of the wing-body configuration at zero angle of attack and sideslip from the coefficients for the model with nacelles.

Accuracy

The estimated accuracy of the measurements is as follows:

	M = 0.4	M = 0.9
C_D	±0.0009	±0.0003
C_L	±0.01	±0.003
C_l	±0.0015	±0.0005
C_m	±0.0007	±0.0002
C_n	±0.003	±0.0008
C_Y	±0.0018	±0.0005
C_F	±0.05	±0.05
$C_{p,b}$	±0.01	±0.004
M	±0.005	±0.005
α, deg	±0.1	±0.1
β, deg	±0.2	±0.2
δ and θ, deg	±0.1	±0.1
$p_{t,j}/p$	±0.05	±0.05

RESULTS

The results of the investigation are presented in the following figures:

Power Off

Power On

Aerodynamic characteristics with nacelles deflected for longitudinal control:

DISCUSSION

Aerodynamic Characteristics, Power Off

Wing-body configuration.- With a leading-edge sweep of $25°$, the streamwise thickness-to-chord ratio for the outer wing panel is 0.127 and, as shown in figure 8, the wing-body configuration exhibits characteristics typical of thick airfoil sections in this speed range. The pitching-moment curves (fig. 8(b)) indicate the onset of static instability at a lift coefficient of about 0.4 for Mach numbers up to 0.80. At a Mach number of 0.90, the peculiarities in the lift and pitching-moment curves at low angles of attack are due to reversals in loading over the rear portion of the thick airfoil. (See ref. 7.) The lift-drag ratios (fig. 8(c)) at Mach numbers of 0.4 and 0.6 reach a maximum value of about 19 at a lift coefficient of 0.3; with increasing Mach number to 0.80 and above, the values of L/D are greatly reduced as would be expected.

Wing-body combination plus nacelles.- For all configurations where nacelles were added to the wing, the swept lateral and vertical fins were mounted on the nacelles as shown in figure 3. The addition of two nacelles below the wing, alined with the airstream, increased the minimum drag coefficient by approximately 15 percent at a Mach number of 0.40 (fig. 9(a)). Adding two nacelles on top of the wing increased $C_{D,o}$ by approximately 37 percent as compared with $C_{D,o}$ for the wing-body combination. Finally, toeing the four nacelles inward $10°$ doubled the minimum drag below a Mach number of 0.6 as compared with the minimum drag of the wing-body combination with nacelles in a streamwise direction. Removal

of the transition strips reduced the value of $C_{D,o}$ of the four-nacelle configuration (10° toe-in) by 0.001 through the Mach number range.

Figure 9(b) shows that below a Mach number of 0.6 adding two nacelles above the wing caused a reduction in maximum lift-drag ratio which was about twice the reduction due to adding two nacelles below the wing. The large losses due to toeing-in the nacelles are again apparent at all test speeds.

It is also shown in figure 9(b) that the longitudinal stability parameter $C_{m_{C_L}}$ was generally reduced slightly by the addition of any combination of nacelles; the lift-curve slope C_{L_α} was also somewhat reduced through part of the Mach number range for all nacelle configurations.

Nacelle deflection for longitudinal control.- The aerodynamic characteristics of the model with the nacelles deflected in the vertical plane as a pitch-control device are presented in figure 10. The pitching-moment curves for the undeflected nacelles ($\theta = 0$) indicate that the lift coefficient at the onset of static instability is only slightly greater than that for the wing-body combination alone (fig. 8(b)).

Previous work, for example, references 4 and 8, indicated that aerodynamic pitch control obtained by deflecting nacelles alone (no fins) was trivial. The results of this investigation show the ineffectiveness of the nacelles with fins as a longitudinal trimming device. It can be seen in figures 10(c) and 11(a) that with the maximum deflection of the control in these tests ($\theta = -15^\circ$) the model could be trimmed only up to a lift coefficient of about 0.2. Also, the onset of instability shifts to a lower lift coefficient as the nacelle pitch deflection is increased in the negative direction, thus compounding the difficulty of trimming to a high lift coefficient. The low values of the pitch-control power parameter C_{m_θ} shown in figure 11(b) result primarily from the small moment arm available with a wing sweep of 25°. (See fig. 1.) The C_{m_θ} values of this investigation show good agreement with those of reference 4 in which are reported results for a configuration similar to the one of the present tests except that the wing was twisted and cambered for a supersonic Mach number.

Lateral and Directional Characteristics, Power Off

Nacelle deflection for directional control.- The lateral and directional characteristics of the model with the nacelles deflected in the

lateral plane as a directional control device are shown in figure 12. Except for small variations above a lift coefficient of about 0.5, where separation occurs on the wings, the yawing-moment coefficient is essentially constant with increasing lift coefficient both at $\beta = 0°$ and $10°$ (fig. 12(a)). The effectiveness of the nacelle-fin combinations as rudder controls and the variation of the rudder-control power parameter $C_{n_{\Delta\delta}}$ with Mach number are shown in figure 13. The swiveling pylon-nacelle-fin control is shown to suffer little loss in effectiveness because of either increasing Mach number or increasing lift coefficient. However, it should be pointed out that as much as 40 percent of the yawing moment can be attributed to an increase in drag on the two nacelles of one wing over that of the two nacelles on the opposite wing. This large drag contribution to directional control is, of course, not present in the case of conventional rudders, nor would it be available for the present configuration if the neutral position of the nacelles were straight ahead.

At $\beta = 0°$ and at Mach numbers of 0.4 and 0.6, figure 12(c) shows that C_l generally has the same sign as C_n for various yaw control deflections. Reversals of this favorable roll due to rudder deflection occur at low values of lift coefficient for a Mach number of 0.80, which are apparently due to shock-wave-induced separation on the thick airfoil section. Similarly, differences in flow separation on the two wings at the higher values of C_L cause some fairly rapid changes in rolling-moment coefficient, particularly for neutral or positive rudder deflections. The direction of these changes indicates that separation was occurring on the right wing at slightly lower angles of attack than was the case for the left wing.

Nacelle deflection for lateral control.- The lateral and directional characteristics for the model with the nacelles deflected differentially in the vertical plane for lateral control are presented in figure 14. With increasing angle of attack, there was generally a slight decrease in C_l and a small increase in adverse yawing moments. The results shown in figure 15 indicate essentially linear variation of C_l with nacelle deflection and relatively small effects of either angle of attack or Mach number. At zero angle of attack, the roll-control power parameter $C_{l_{\Delta\theta}}$ was approximately 0.0007 and 0.0006 at Mach numbers of 0.40 and 0.60, respectively.

Stability characteristics.- The variation of yawing-moment coefficient with angle of sideslip (fig. 16(a)) indicates a slight decrease in slope above $\beta = 6°$. The directional stability parameter C_{n_β} is shown in figure 16(b) to be stable throughout the Mach number range and to increase slightly with increasing lift coefficient. The values of C_{n_β}

for the uncambered wing of the present tests were about the same as those shown at low speeds for a similar model with a cambered wing (ref. 4).

<div align="center">Aerodynamic Characteristics, Power On</div>

The jet total-pressure ratios shown in this paper are the averages for the four engines except for the one-engine-out condition, where the jet total-pressure ratio is the average for the two engines on the wing opposite the inoperative engine. The engine on the same wing as the inoperative one had a total-pressure ratio about 20 percent higher than the average of the other two. It should be noted that for the Swallow engines, which were simulated in these tests, the total-pressure ratios (average for altitudes from sea level to tropopause) for maximum continuous thrust at Mach numbers of 0.40, 0.60, and 0.80 are approximately 2.0, 2.5, and 3.0, respectively.

A comparison of the results obtained with the flow-through nacelles and the jet-off results obtained with the hot-jet (faired-nose) nacelles indicated some small differences in drag coefficients but insignificant differences in any of the control characteristics.

Nacelles deflected for longitudinal control.- The model aerodynamic characteristics with the jet thrust components included are shown in figure 17 for several nacelle pitch deflections. Only at the lowest Mach number of the tests (M = 0.40) did jet operation provide any significant increase in pitch control effectiveness as indicated by the variation of pitching-moment coefficient with jet pressure ratio (fig. 17(c)). It is not too surprising, therefore that the loss of power on one engine had only a slight effect on the longitudinal stability.

The force and moment coefficients in figure 18 have had the calculated components of jet thrust removed and are thus composed only of the aerodynamic and jet interference effects. The jets-on lift and pitching-moment coefficients are nearly identical to the jets-off points $\left(p_{t,j}/p = 1.0\right)$ indicating that the jet-induced effects on these components are trivial. The drag coefficients, however, do show a change with jet operation; these effects are shown as incremental drag (jets-on minus jets-off) in figure 19. The favorable drag effects $\left(-\Delta C_{D,j}\right)$ shown at some test conditions are believed to be due to the jet pumping action cleaning up a poor flow field (separation) associated with the 10° toe-in of the pylon-nacelle-fin arrangement.

Lateral and Directional Characteristics, Power On

Nacelles deflected for directional control.- The lateral and direc-
tional characteristics (components of jet thrust included) of the model
with nacelles deflected for directional control are presented in fig-
ure 20 for an angle of attack of 4° and angles of sideslip of 0° and 5°.
Because of the fairly long yawing-moment arm involved (0.61 b/2), one-
engine-out operation had an appreciable effect on C_n; however, the
rudder control power is sufficient to trim for this unbalanced thrust
condition with 2° or 3° change in nacelle deflection. With the compo-
nents of jet thrust removed (fig. 21), the data indicate that the jet
interference effects are generally negligible. One exception is yawing-
moment coefficient at 5° sideslip angle where it appears that the jet
effects would cause some increase in the value of C_{n_β}.

Nacelles deflected for lateral control.- The lateral and directional
characteristics (including components of jet thrust) for the model with
nacelles deflected differentially in the pitch plane for lateral control
are presented in figure 22. The increase in rolling-moment coefficients
with jet pressure ratio is just the amount calculated by applying the
thrust vectors at the proper moment arms; thus, as indicated in figure 23
(data with thrust components removed), there were essentially no jet
interference effects on C_l. There was, however, some increase in the
adverse yawing moments due to jet interference effects.

SUMMARY OF RESULTS

An investigation of the performance, stability, and control char-
acteristics of a variable-sweep arrow-wing model ("Swallow") with the
outboard wing panels swept 25° indicates the following results:

1. The basic wing-body configuration exhibited longitudinal insta-
bility at relatively low lift coefficients; the addition of the unde-
flected nacelles and fins delayed the onset of instability to only
slightly higher values of lift coefficient.

2. At Mach numbers below 0.6 the addition of two nacelles on the
upper wing surfaces of the wing-body configuration caused a reduction
in maximum lift-drag ratio which was about twice as great as adding two
nacelles below the wing.

3. The minimum drag coefficient for the model with the nacelles
toed-in 10° was double that for the model with nacelles alined with the
free stream for Mach numbers below 0.6; the maximum lift-drag ratio was
correspondingly greatly reduced.

4. The nacelle-fin combinations were ineffective for longitudinal control largely because of the small moment arm available with 25° wing sweep.

5. The pylon-nacelle-fin combinations were effective as directional controls; however, approximately 40 percent of the yawing moment was due to the increased drag of the deflected nacelles.

6. The nacelle-fin combinations provided adequate lateral control and were relatively unaffected by increasing either Mach number or angle of attack.

7. The directional stability for the present model with an uncambered wing increased with lift coefficient and was about the same as that of a similar model having a cambered wing.

8. The jet interference effects on the model stability and control characteristics were generally small; the effects on drag were appreciable, particularly at a Mach number of 0.40. At some test conditions the effects on drag were favorable.

9. Loss of power on one engine had little effect on longitudinal stability; the effects on directional stability were larger but could be controlled with small deflection of the nacelles.

Langley Research Center,
    National Aeronautics and Space Administration,
        Langley Field, Va., March 22, 1960.

SECRET

REFERENCES

1. Finch, Thomas W., and Briggs, Donald W.: Preliminary Results of Stability and Control Investigation of the Bell X-5 Research Airplane. NACA RM L52K18b, 1953.

2. Wallis, B. N.: A Note on a Proposed New Type of Aircraft. Vickers-Armstrongs (Aircraft), Ltd. (Weybridge, England).

3. Anon.: The "Swallow" Project - Proposal for a Research Aircraft Capable of Wide Military Applications (Including Strike Reconnaissance Duties). Preliminary Drawings, Vickers-Armstrongs (Aircraft), Ltd. (Weybridge, England).

4. Harris, R. M.: Low Speed Wind Tunnel Tests of a Cambered and Twisted Model of the Swallow With 25° Sweep of the Leading Edge of the Afterwings. Rep. No. RD 011/1, Vickers-Armstrongs (Aircraft), Ltd. (Weybridge, England).

5. Runckel, Jack F., and Swihart, John M.: A Hydrogen Peroxide Hot-Jet Simulator for Wind-Tunnel Tests of Turbojet-Exit Models. NASA MEMO 1-10-59L, 1959.

6. Braslow, Albert L., and Knox, Eugene C.: Simplified Method for Determination of Critical Height of Distributed Roughness Particles for Boundary-Layer Transition at Mach Numbers From 0 to 5. NACA TN 4363, 1958.

7. Daley, Bernard N., and Dick, Richard S.: Effect of Thickness, Camber, and Thickness Distribution on Airfoil Characteristics at Mach Numbers up to 1.0. NACA TN 3607, 1956. (Supersedes NACA RM L52G31a.)

8. Alford, William J., Jr., and Henderson, William P.: An Exploratory Investigation of the Low-Speed Aerodynamic Characteristics of Variable-Wing-Sweep Airplane Configurations. NASA TM X-142, 1959.

TABLE I

COORDINATES OF RAE 102 AIRFOIL PERPENDICULAR

TO LEADING EDGE

x, percent of chord	y, percent of chord
0 .	0
.10	.518
.50	1.156
.75	1.413
1.25	1.818
2.50	2.549
5.00	3.541
7.50	4.258
10.00	4.823
15.00	5.671
20.00	6.262
25.00	6.663
30.00	6.905
35.00	6.999
40.00	6.935
45.00	6.678
50.00	6.289
60.00	5.251
70.00	4.004
80.00	2.674
90.00	1.337
95.00	.669
100.00	0

(a) Closeup of airflow nacelles.   L-59-4367
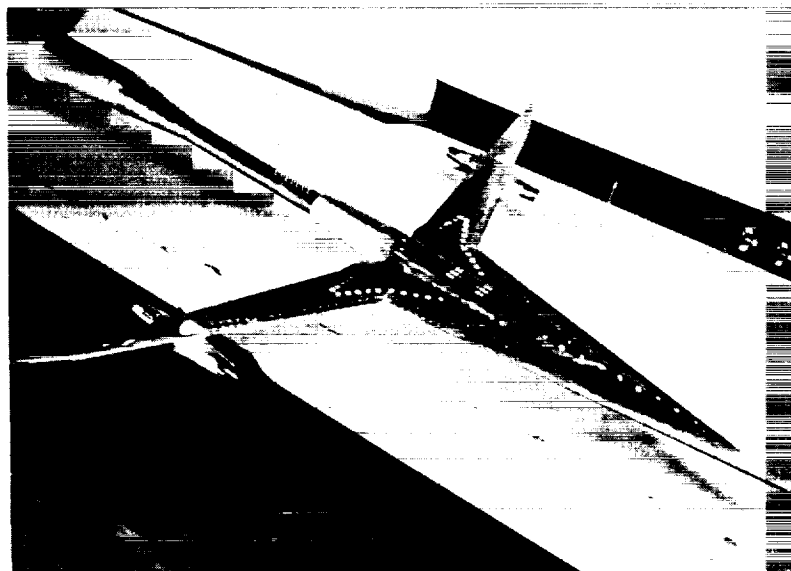
L-59-4699

(b) Model with airflow nacelles mounted below wings.

Figure 2.- Photographs of model with airflow nacelles.

Nacelle Coordinates.					
x	r_1	r_2	x		r_2
.20	0.970	0.954	1.20		0.972
.40	1.027	.991	1.40		.947
.60	1.067	1.013	1.60		.917
.80	1.092	1.014	1.80		.892
1.00	1.107	1.012	2.00		.880
	1.117	.997	2.20		.870
			2.25		.867

Jet-nacelle base pressure location
$\phi = 10°$, 100°, 190°, and 280°
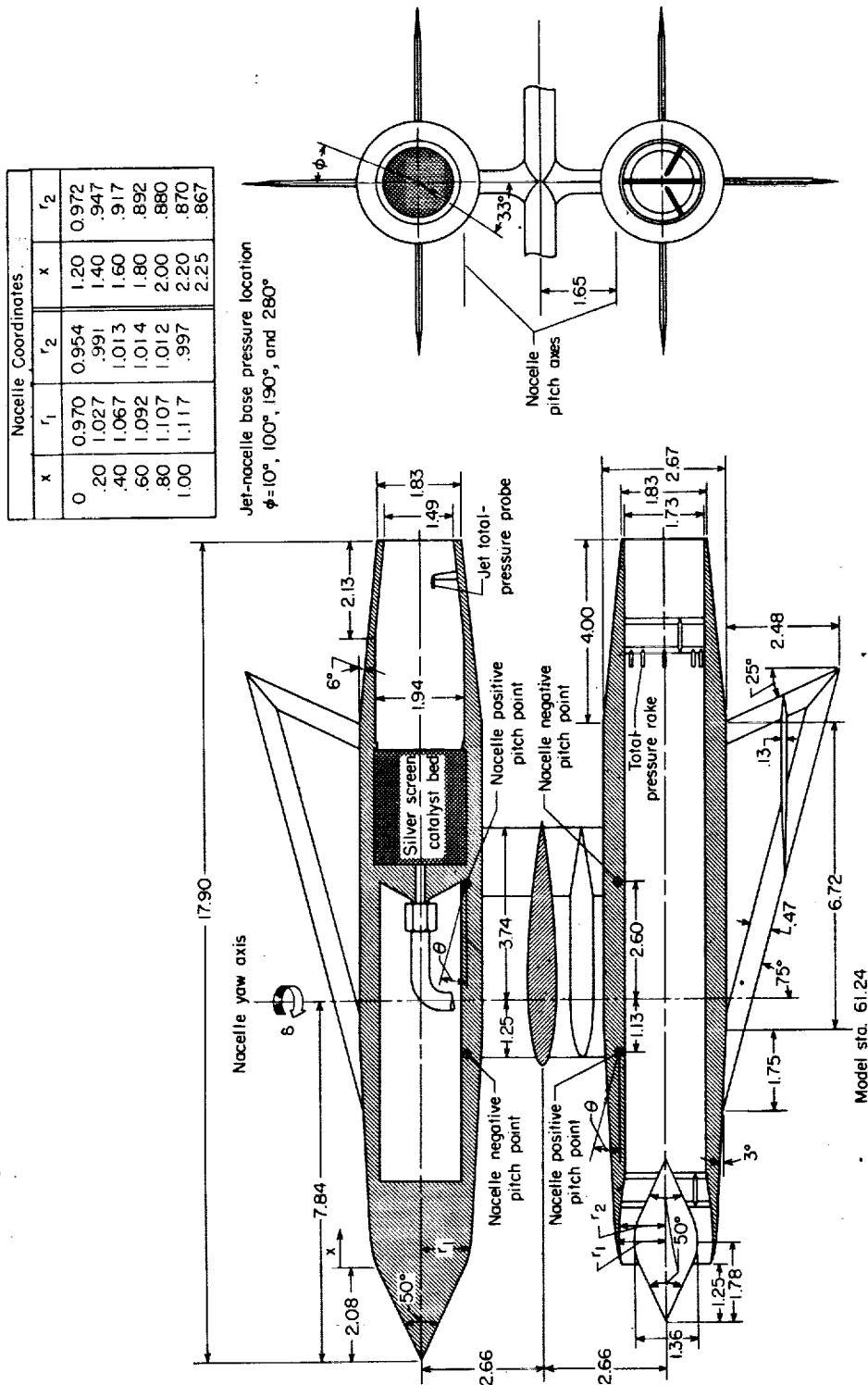
Figure 3.- Sketch showing jet and airflow nacelles, fins, and pylon arrangement. All dimensions are in inches.
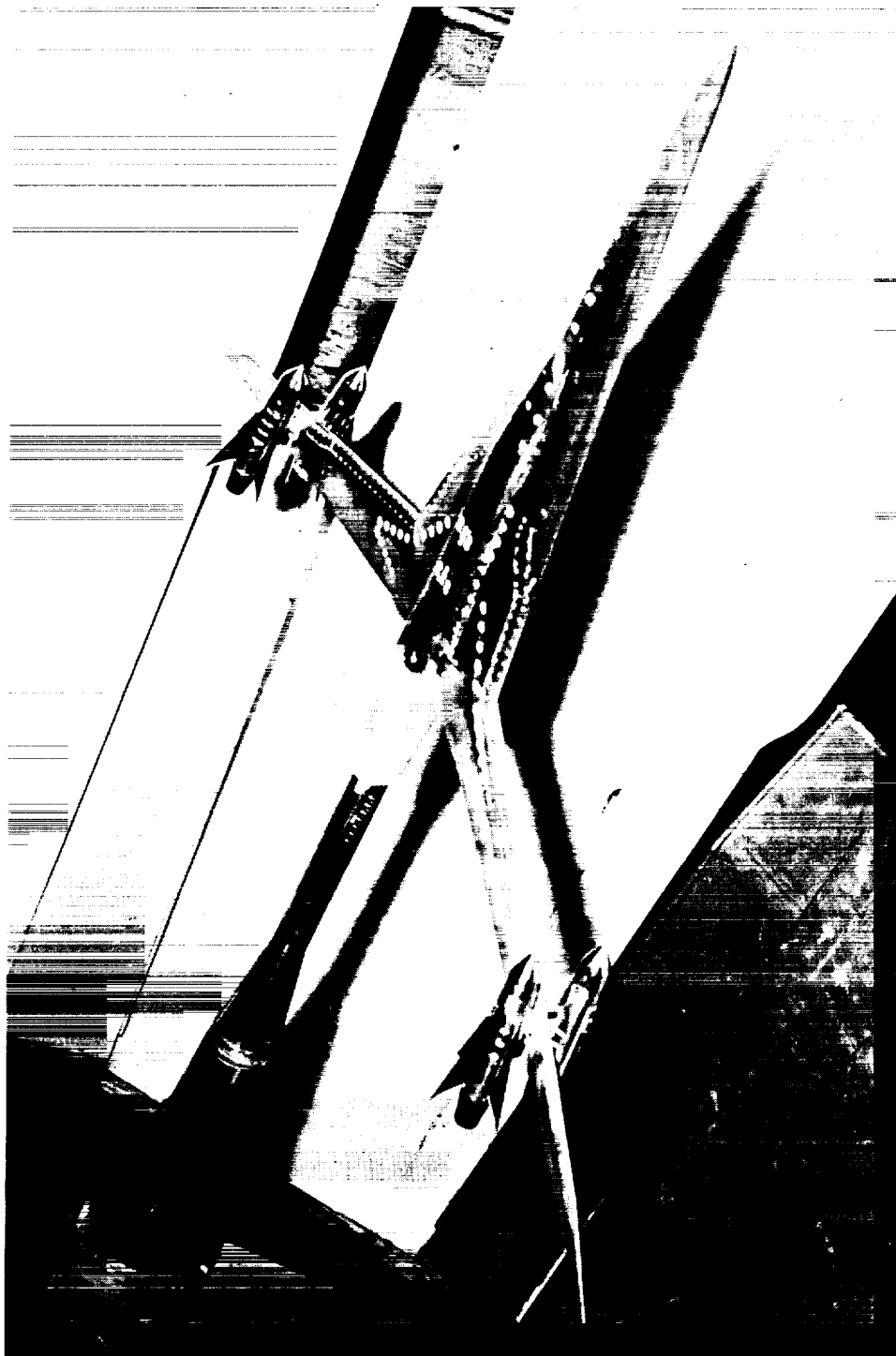
L-59-3772

(a) Nacelle deflection. $\delta_L = 10°$; $\delta_R = -10°$; $\theta = 0°$.

Figure 4.- Photographs of model with jet nacelles.
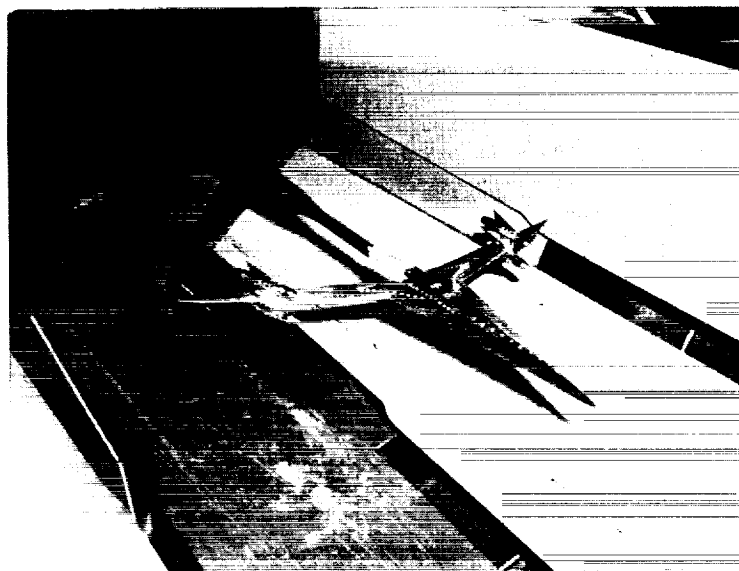
SECRET

L-59-3819

(b) Nacelle deflection. $\delta_L = 0^\circ$; $\delta_R = -20^\circ$; $\theta = 0^\circ$.

L-59-4218
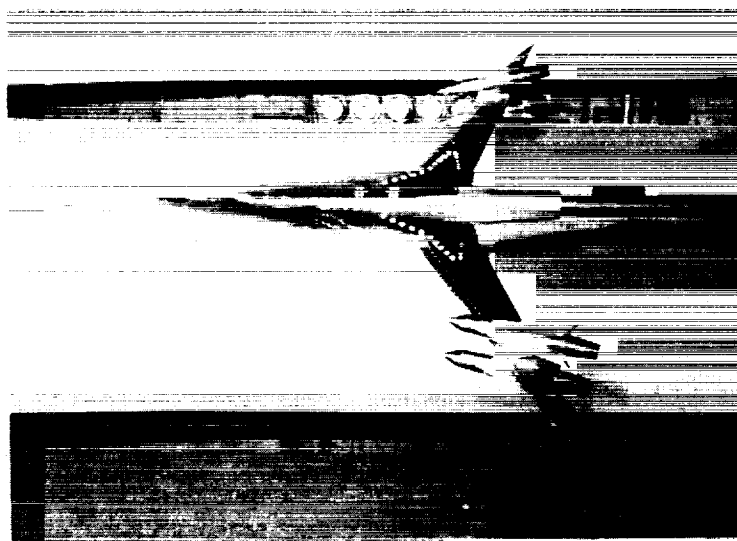
(c) Nacelle deflection. $\delta_L = 10^\circ$; $\delta_R = -10^\circ$; $\theta_L = 15^\circ$; $\theta_R = -15^\circ$.

Figure 4.- Concluded.
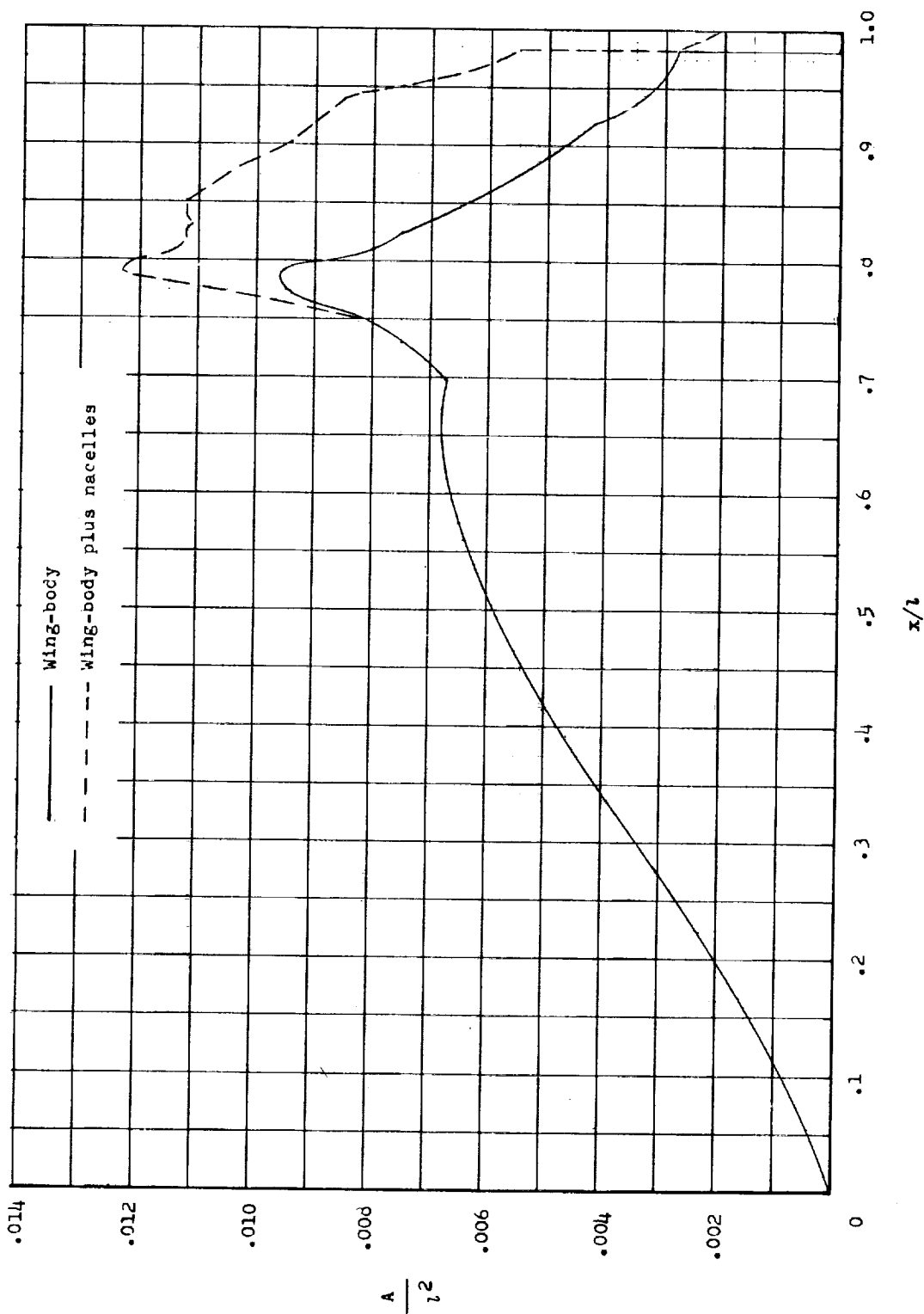
Figure 5.- Area distribution of Swallow variable-sweep-wing model. $\Lambda = 25°$.
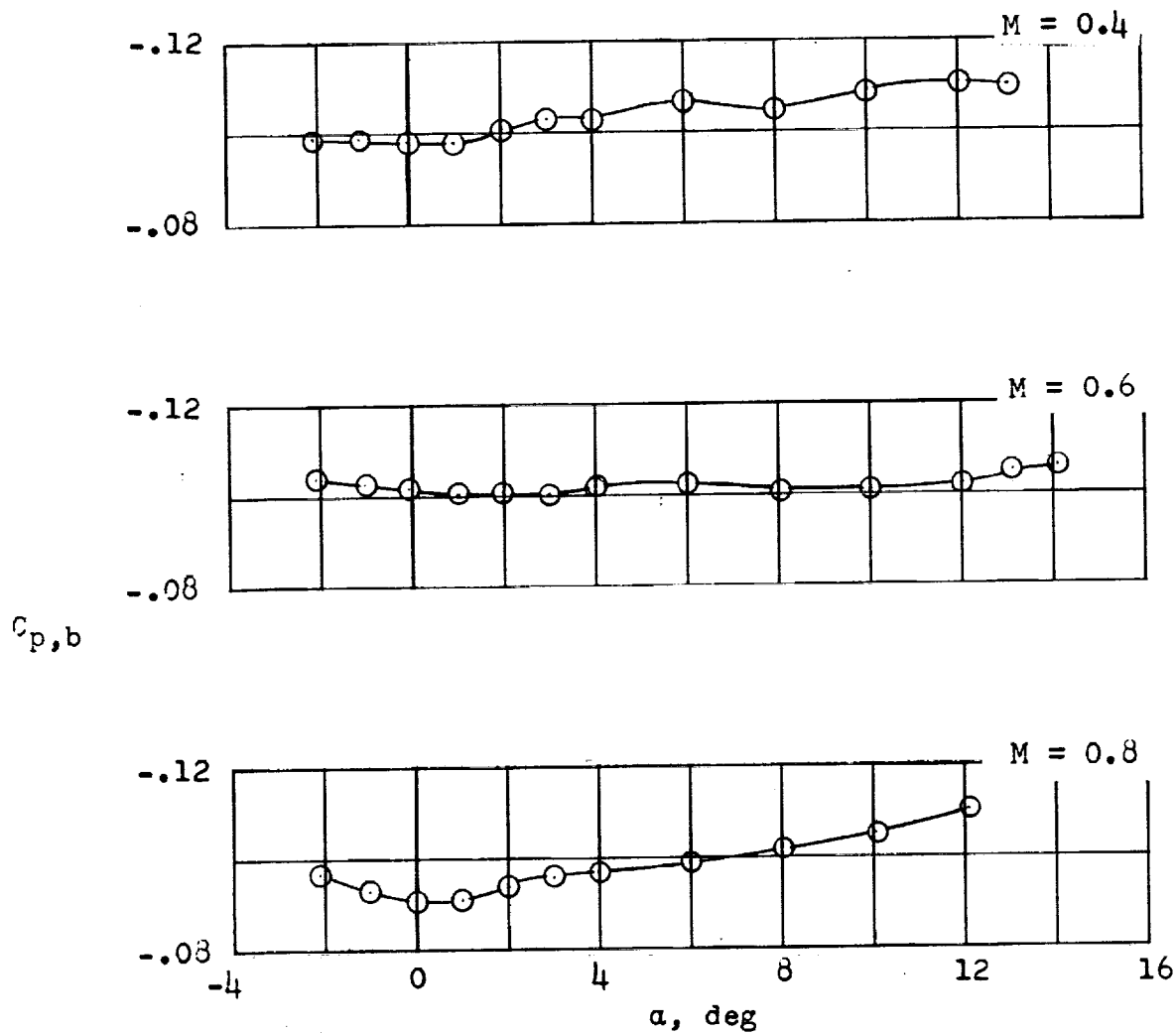
SECRET

(a) Fuselage base pressure coefficient.

Figure 6.- Fuselage base pressure coefficient and internal drag
coefficient. β = 0°.

δ_L, deg	δ_R, deg	θ, deg
10	-10	0.0
10	-10	7.5
10	-10	-15.0
0	-20	0.0
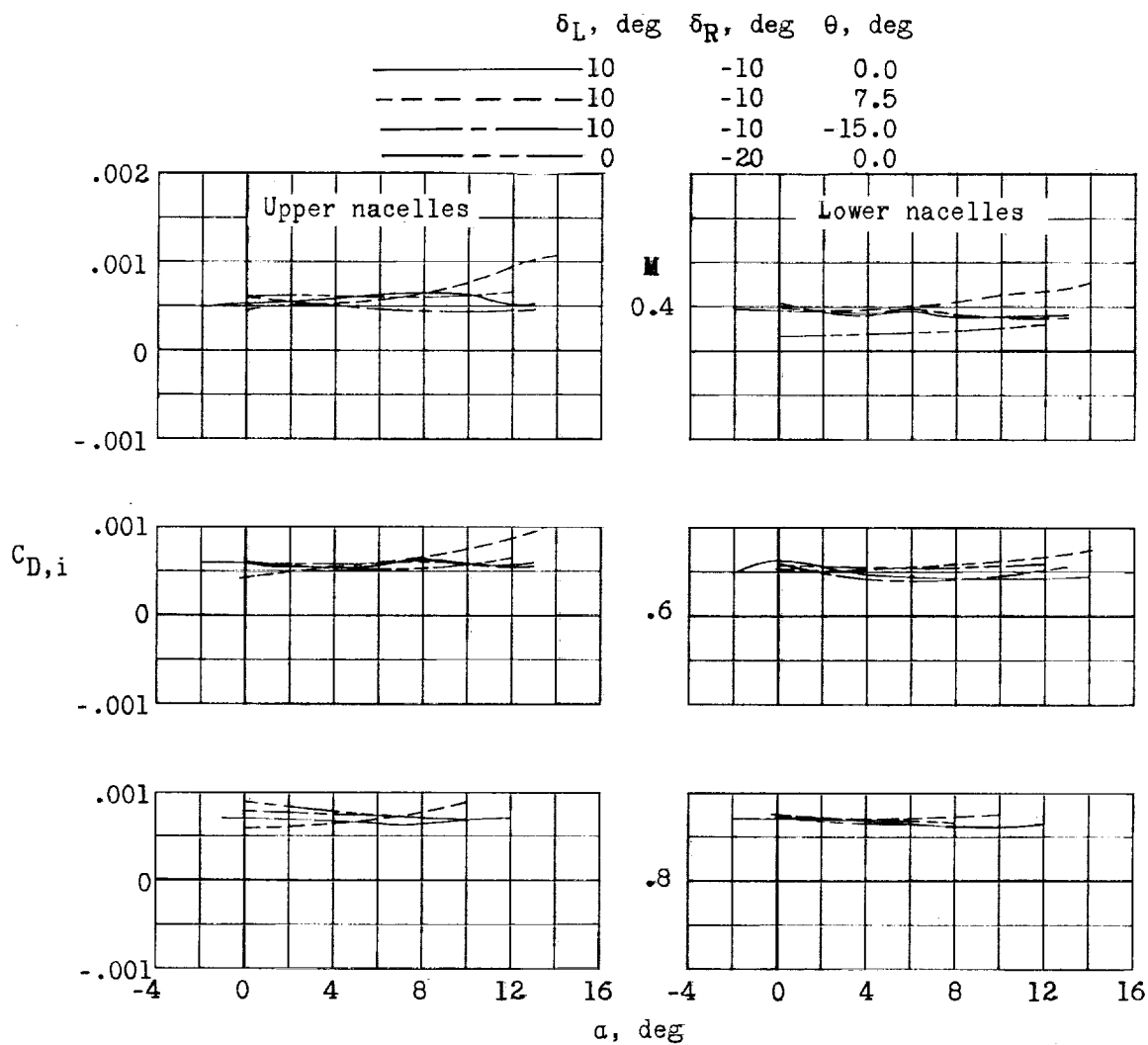
(b) Internal drag coefficient.

Figure 6.- Concluded.

SECRET
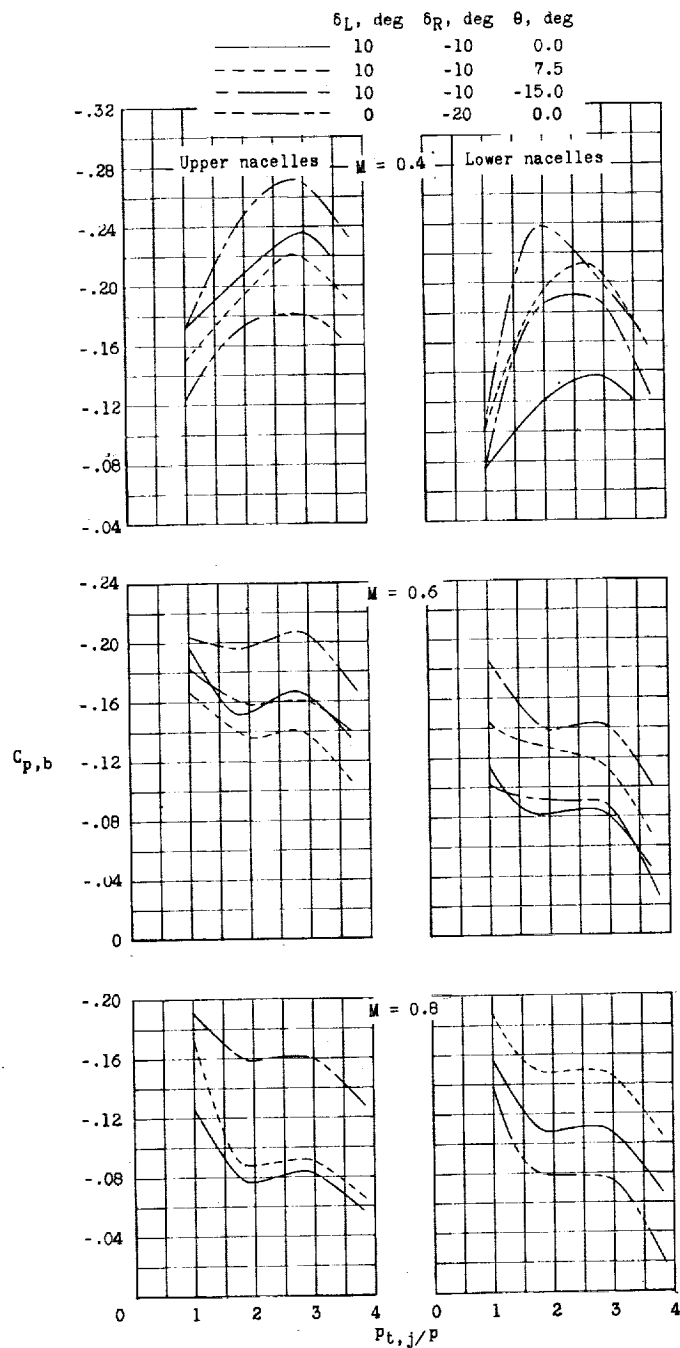
(a) Jet-nacelle base pressure coefficient.

Figure 7.- Nacelle base pressure coefficient and engine
static-jet-thrust calibration. $\alpha = 4°$.
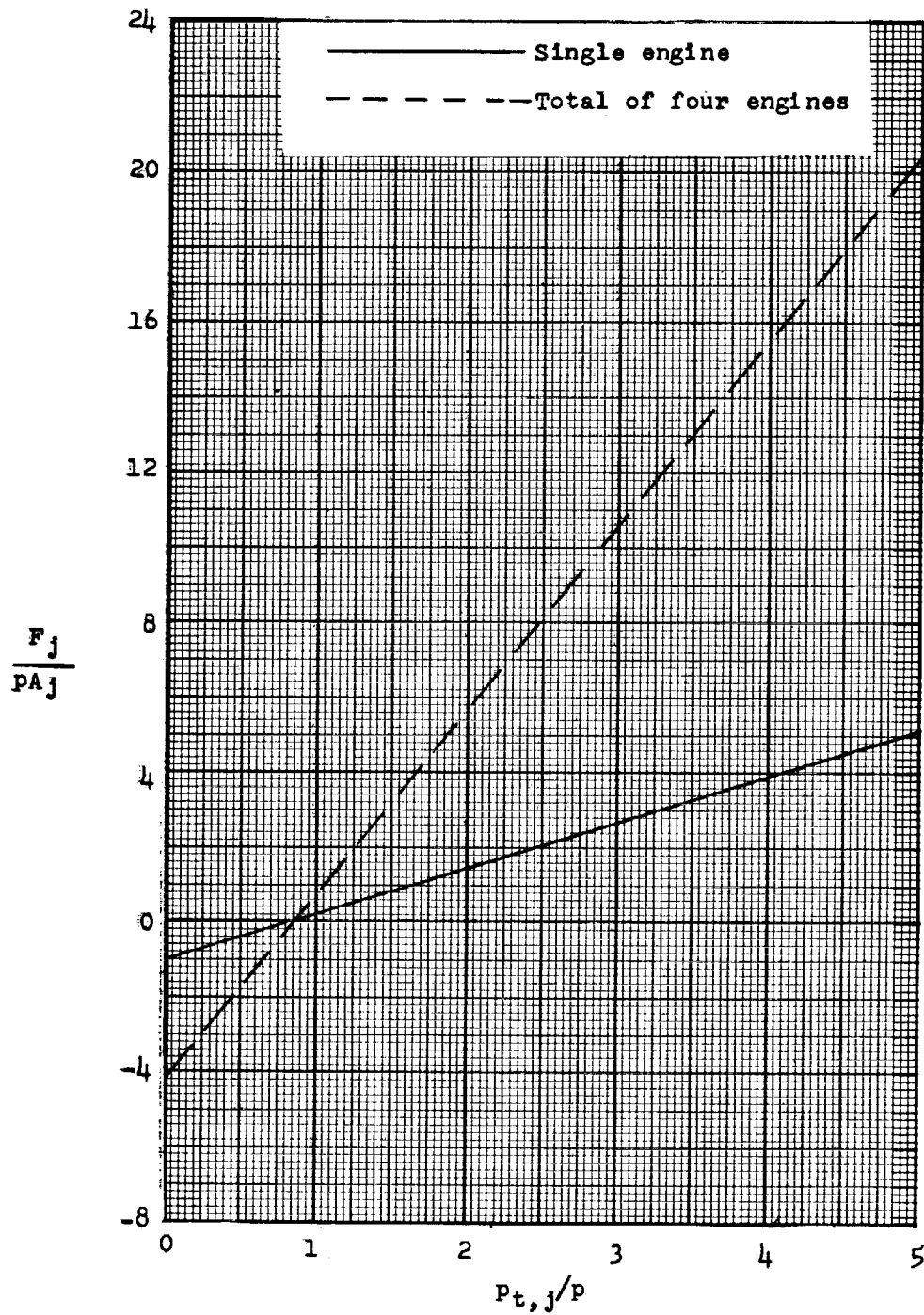
(b) Engine static-jet-thrust calibration.

Figure 7.- Concluded.

SECRET
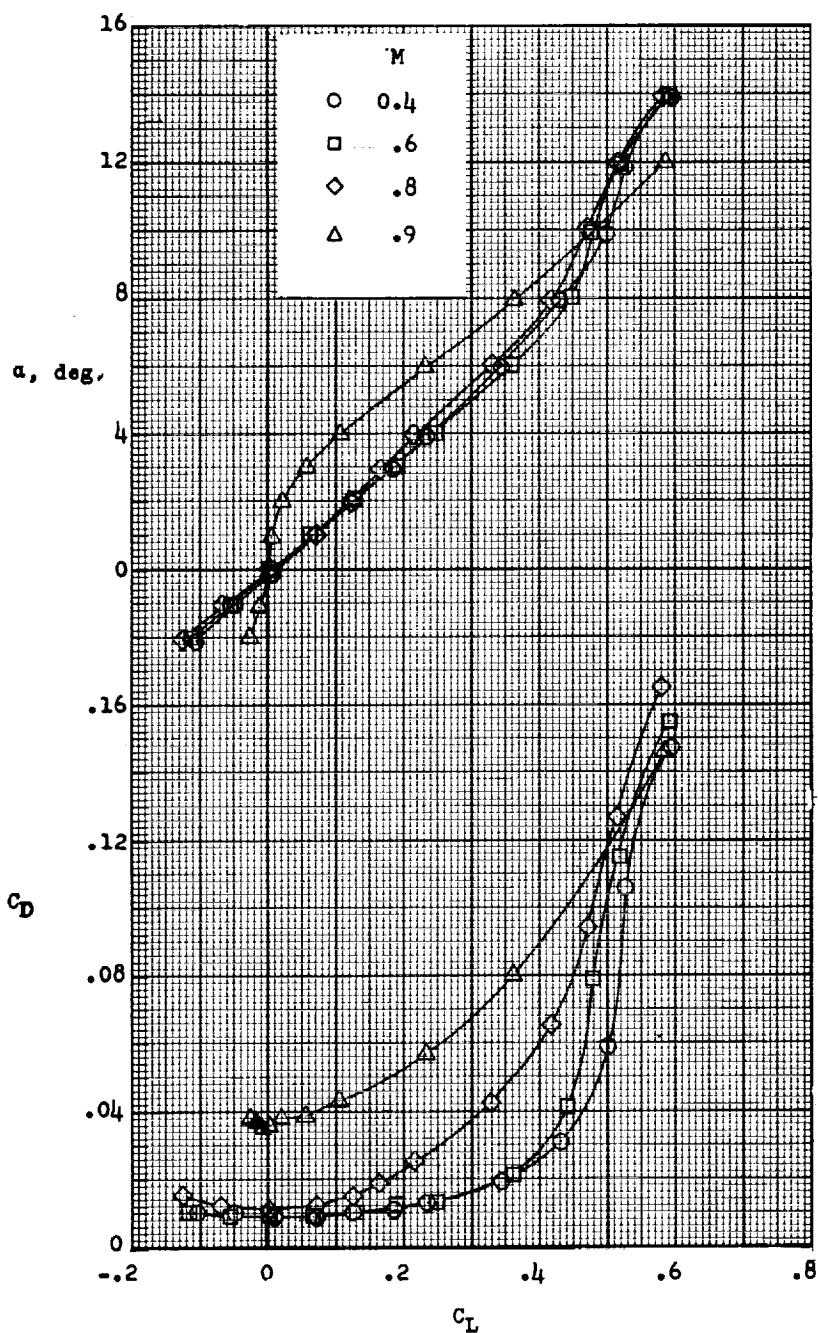
(a) Lift and drag coefficients.

Figure 8.- Aerodynamic characteristics of wing-body combination.
$\Lambda = 25°$; $\beta = 0°$.
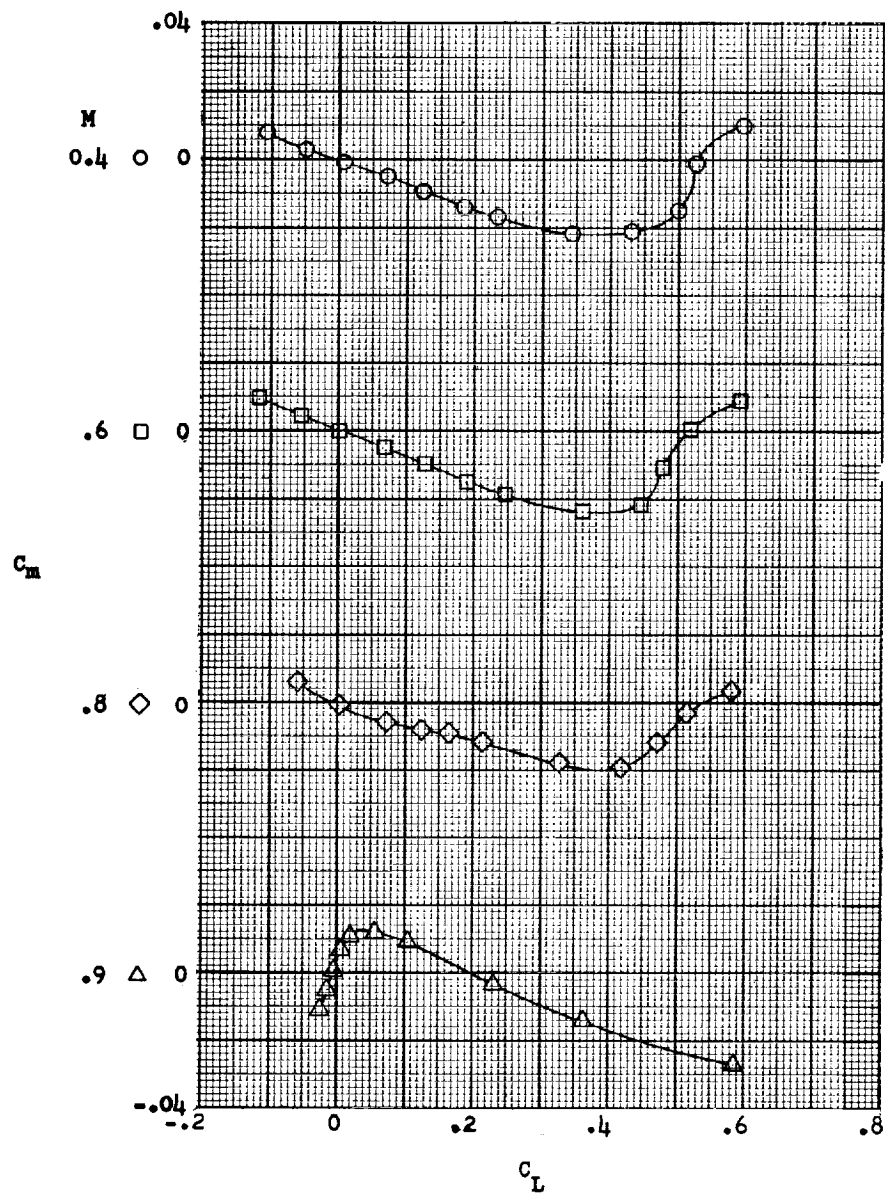
(b) Pitching-moment coefficients.

Figure 8.- Continued.
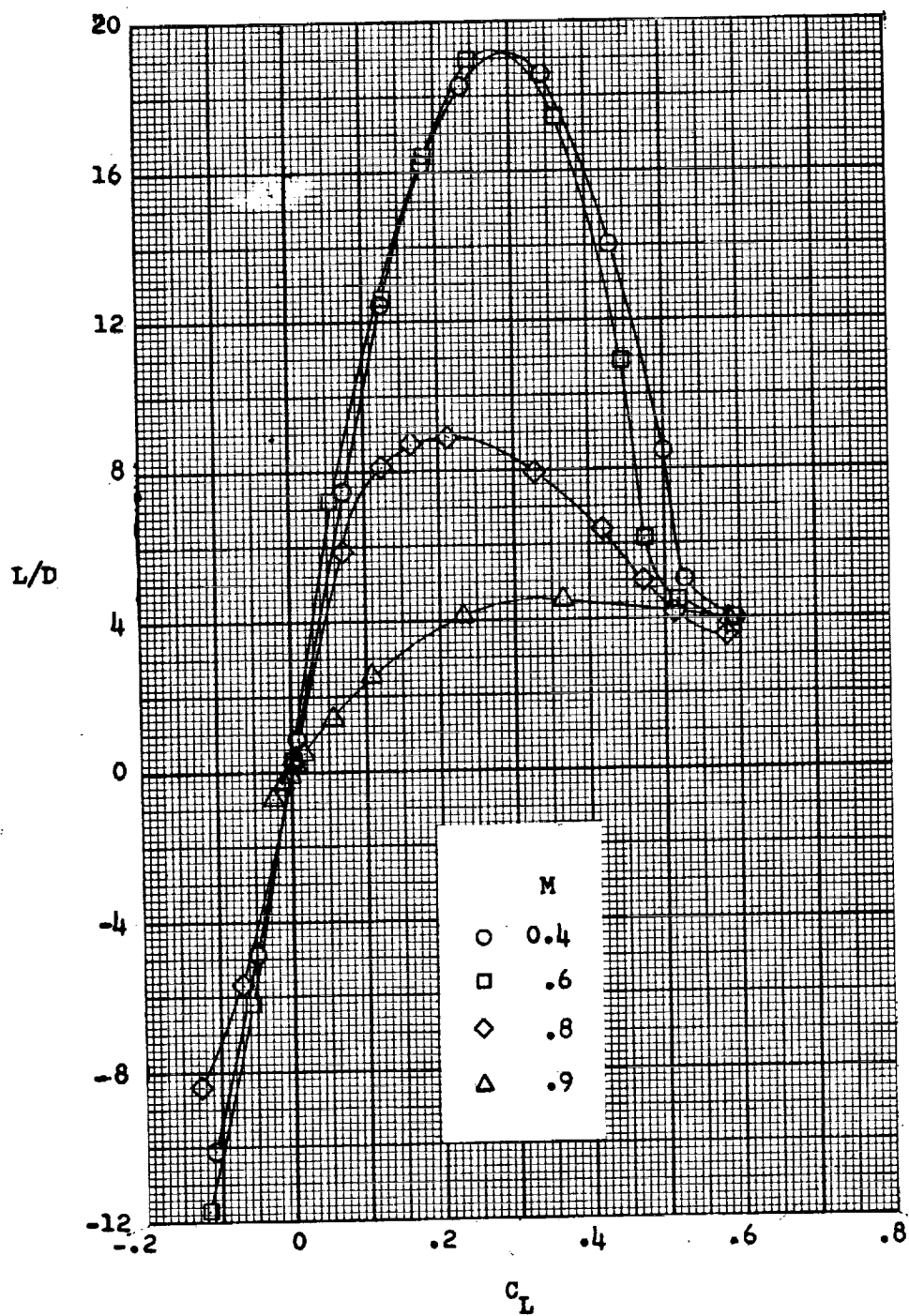
(c) Lift-drag ratios.

Figure 8.- Concluded.

O Wing-body

□ 4 Nacelles, $\delta_L = \delta_R = 0°$

◇ 4 Nacelles, $\delta_L = 10°$, $\delta_R = -10°$

△ 4 Nacelles, $\delta_L = 10°$, $\delta_R = -10°$,
   Without transition

△ 2 Nacelles below wing,
   $\delta_L = \delta_R = 0°$
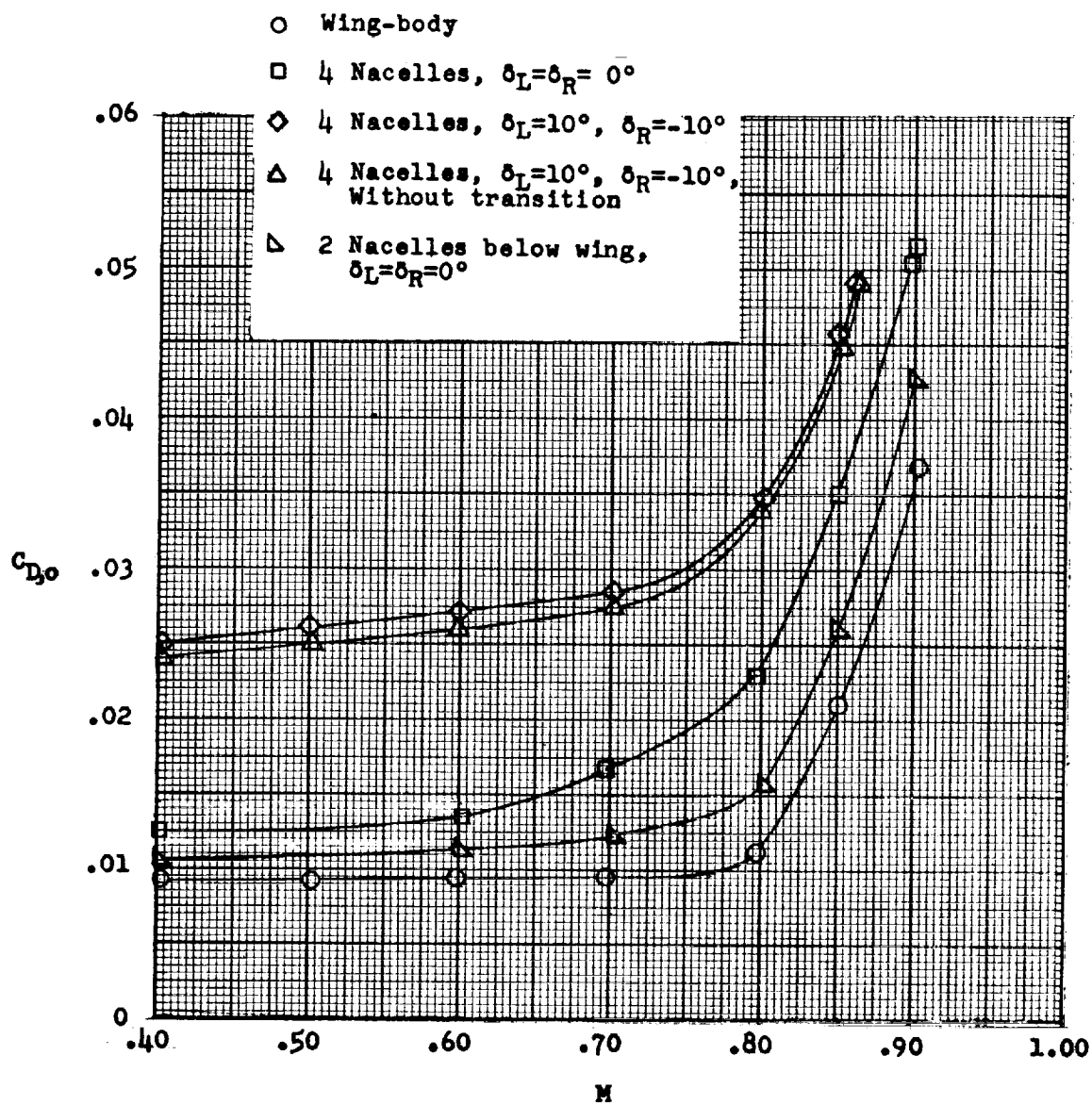
(a) Variation of minimum drag coefficient with Mach number.

Figure 9.- Effect of nacelles on model aerodynamics. $\Lambda = 25°$;
$\beta = 0°$; $\theta_L = \theta_R = 0°$.

SECRET
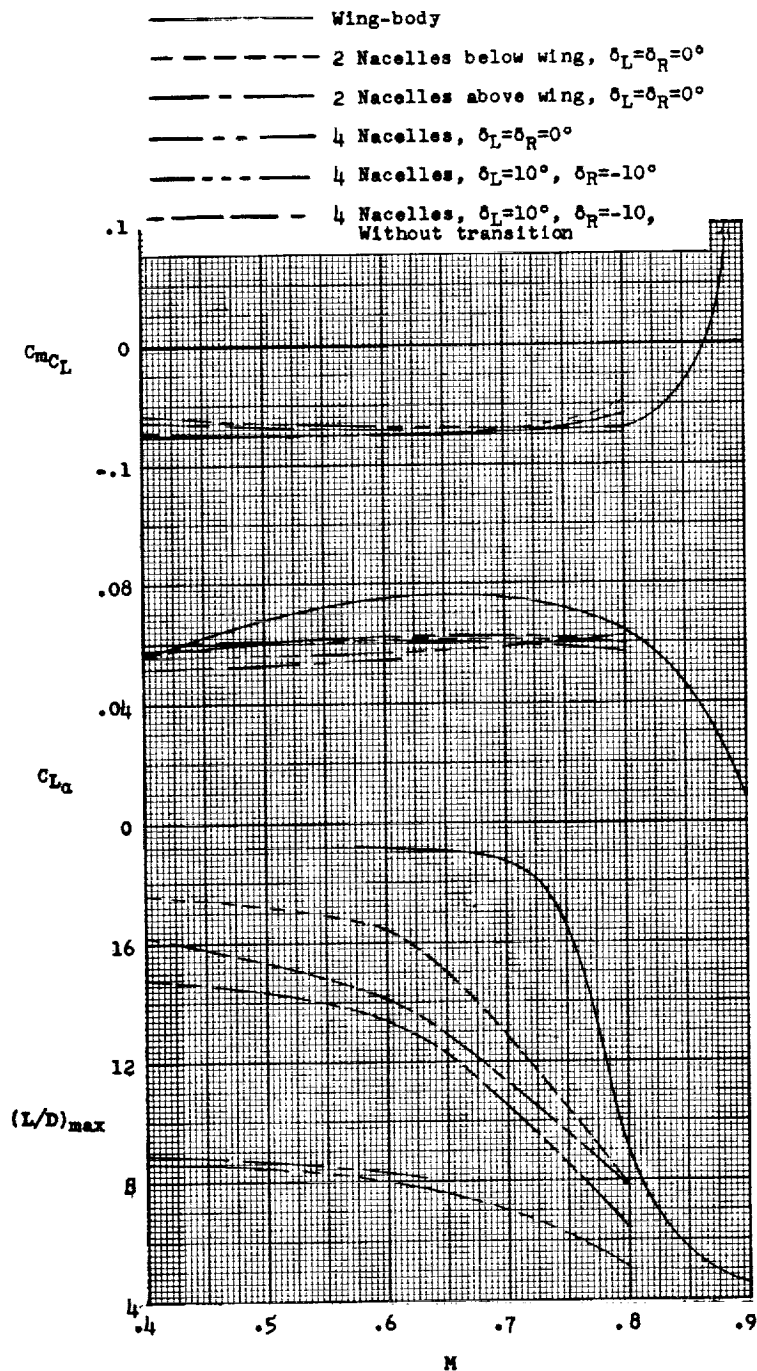
(b) Effect of Mach number on aerodynamic characteristics.

Figure 9.- Concluded.
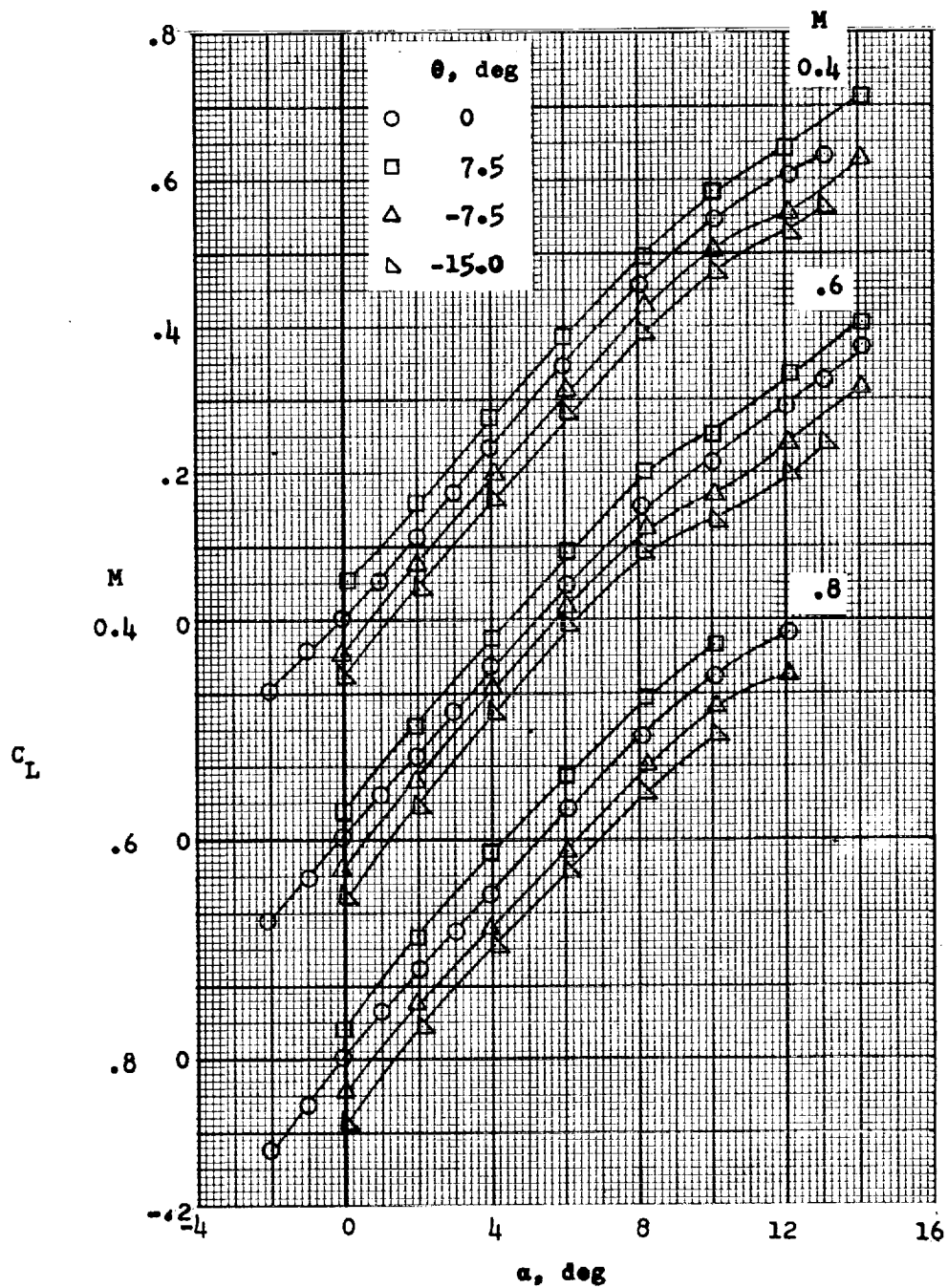
(a) Effect of nacelle pitch deflection on lift coefficient.

Figure 10.- Longitudinal control characteristics.   Airflow nacelles with fins; $\Lambda = 25^\circ$; $\delta_L = 10^\circ$; $\delta_R = -10^\circ$; $\beta = 0^\circ$.
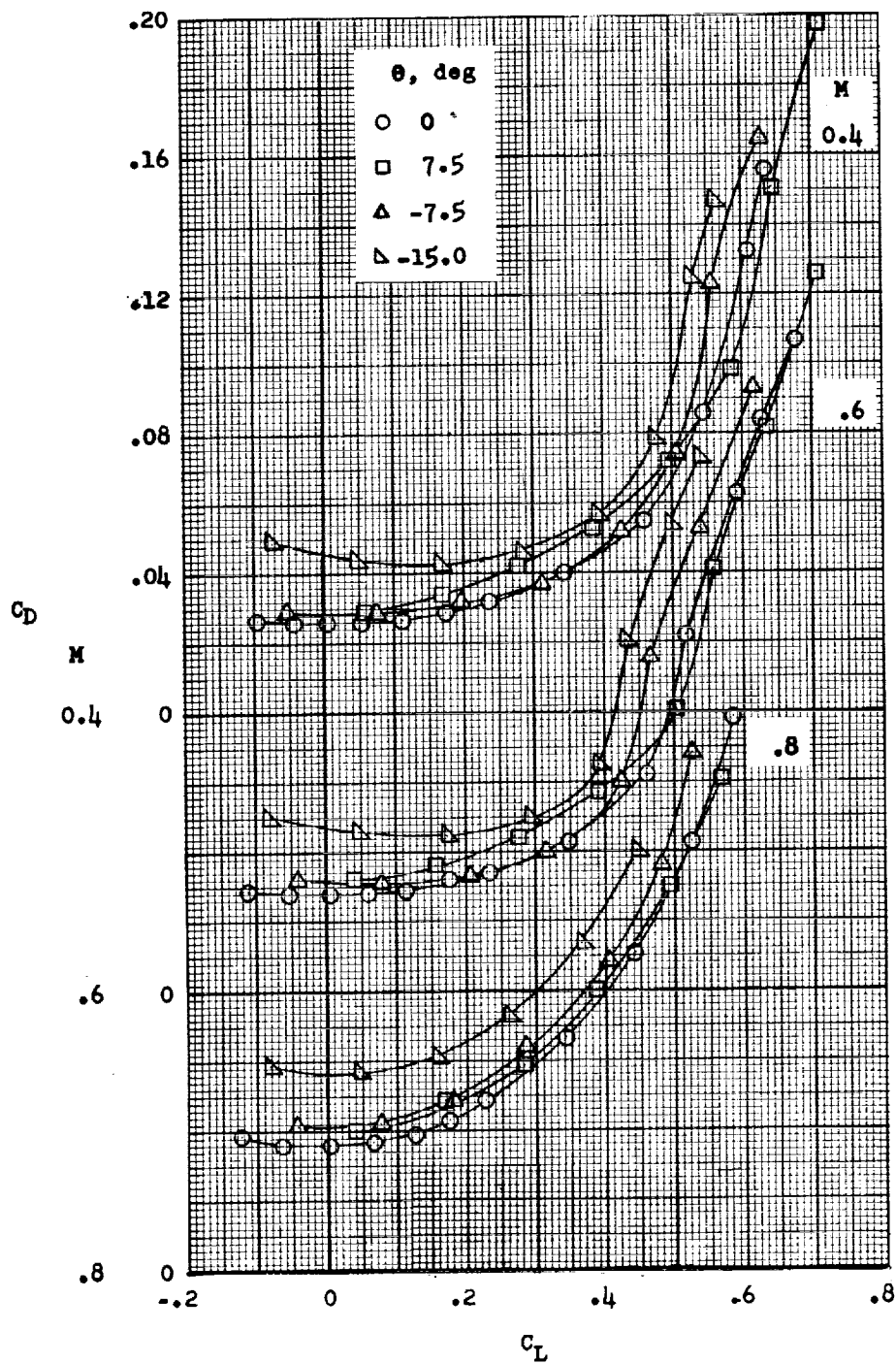
(b) Effect of nacelle pitch deflection on drag coefficient.

Figure 10.- Continued.
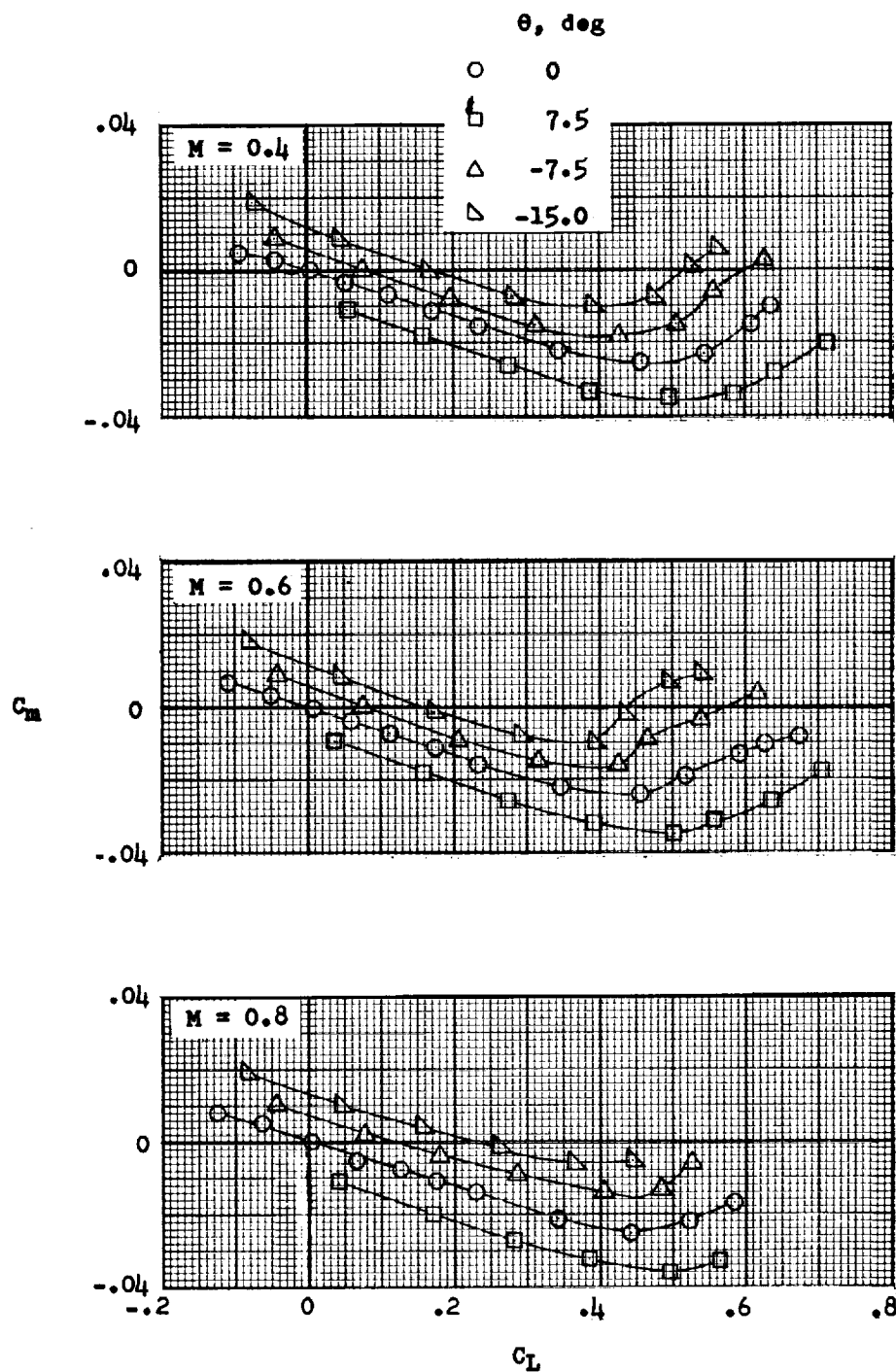
(c) Effect of nacelle pitch deflection on pitching-moment coefficient.

Figure 10.- Concluded.
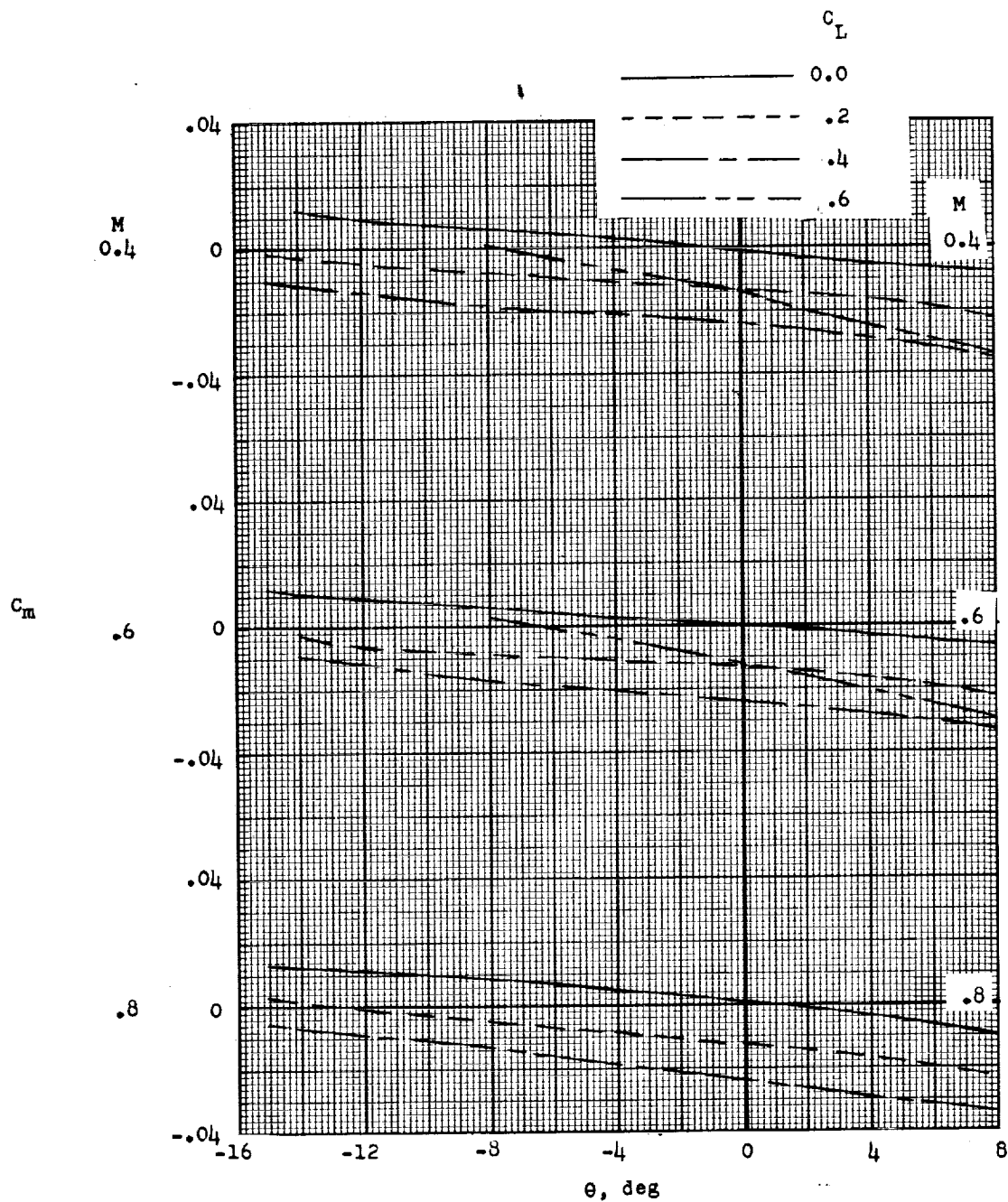
(a) Variation of C_m with θ.

Figure 11.- Longitudinal control effectiveness. Airflow nacelles with fins; $\Lambda = 25^\circ$; $\delta_L = 10^\circ$; $\delta_R = -10^\circ$; $\beta = 0^\circ$.
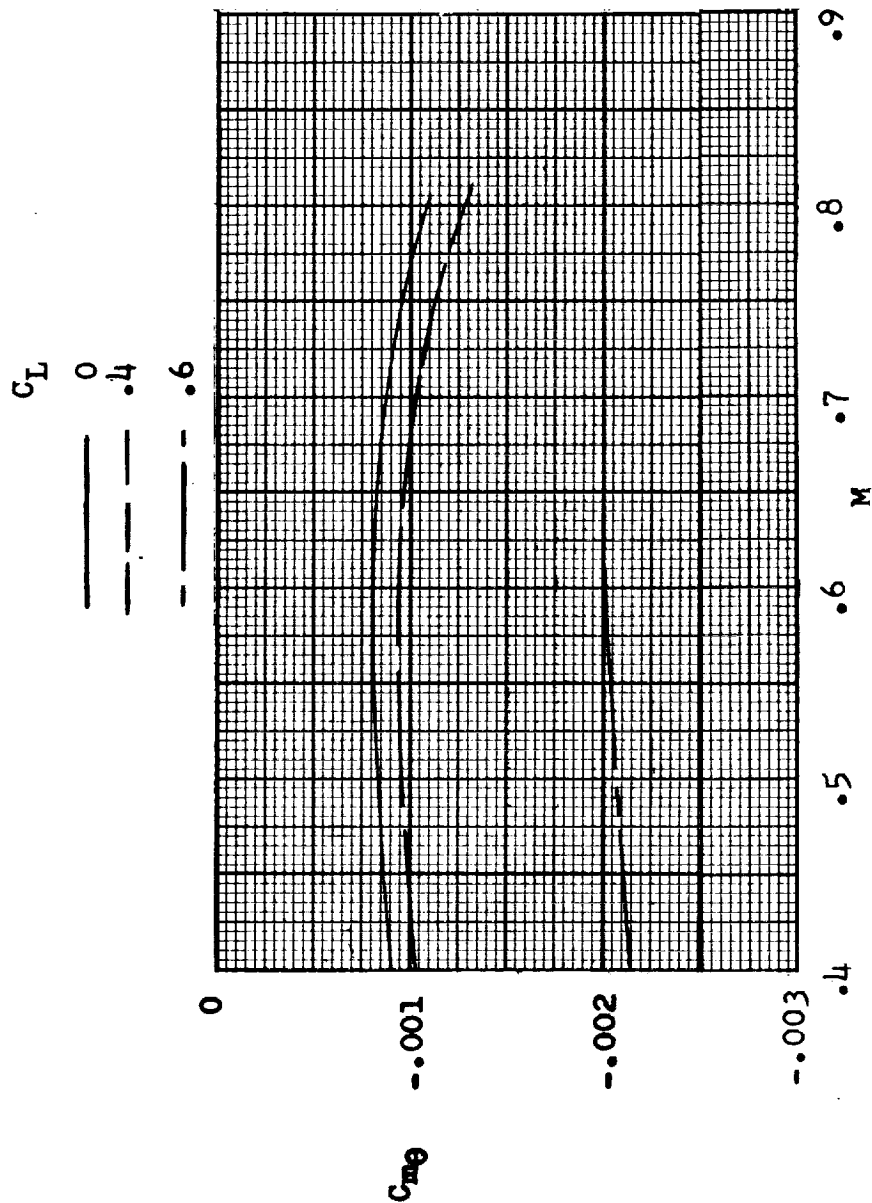
(b) Variation of C_{m_θ} with M.

Figure 11.- Concluded.
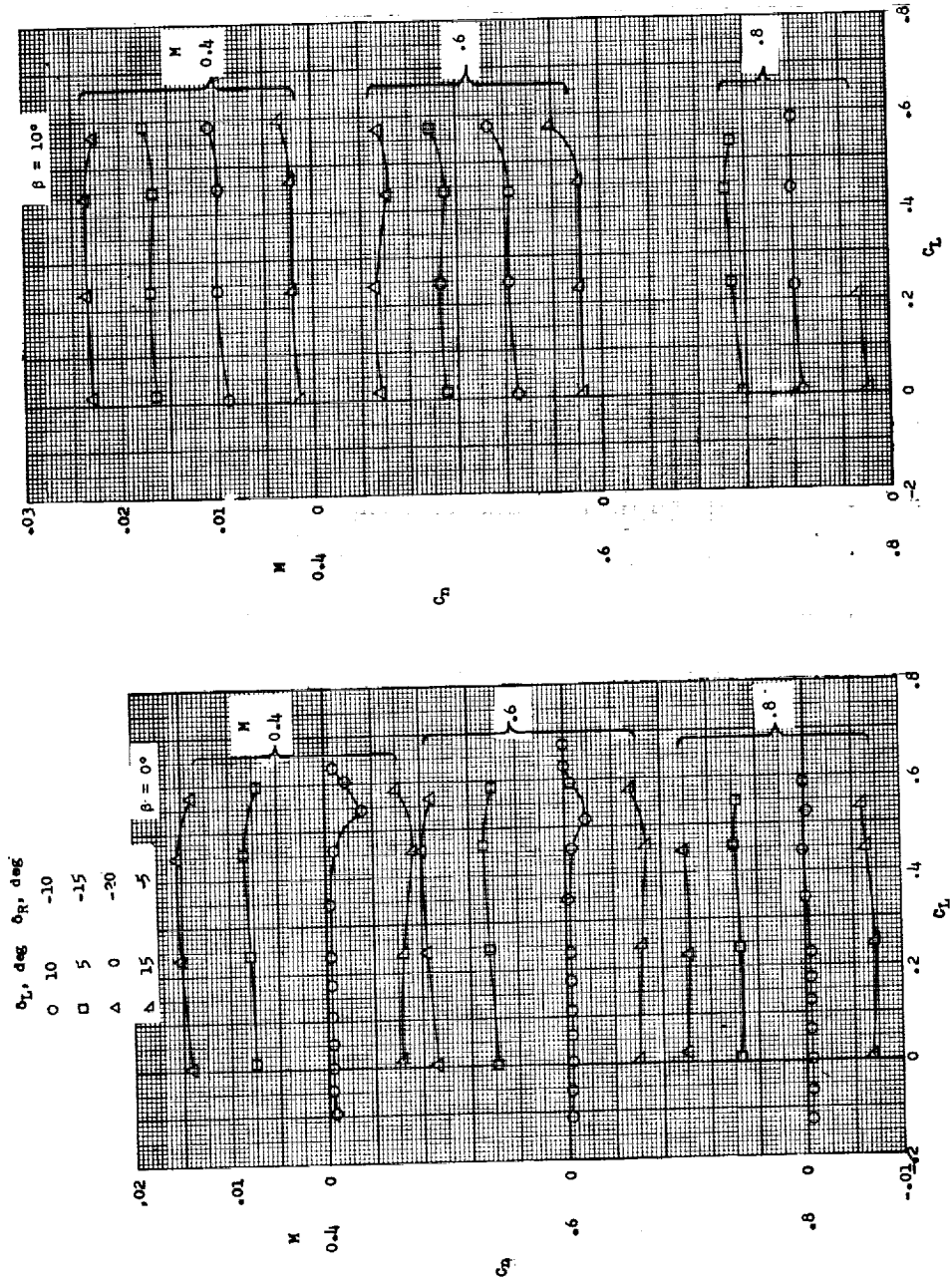
(a) Effect of nacelle yaw deflection on yawing-moment coefficient.

Figure 12.- Directional control characteristics. Airflow nacelles with fins; $\Lambda = 25°$; $\theta_L = \theta_R = 0°$; $\beta = 0°$ and $10°$.
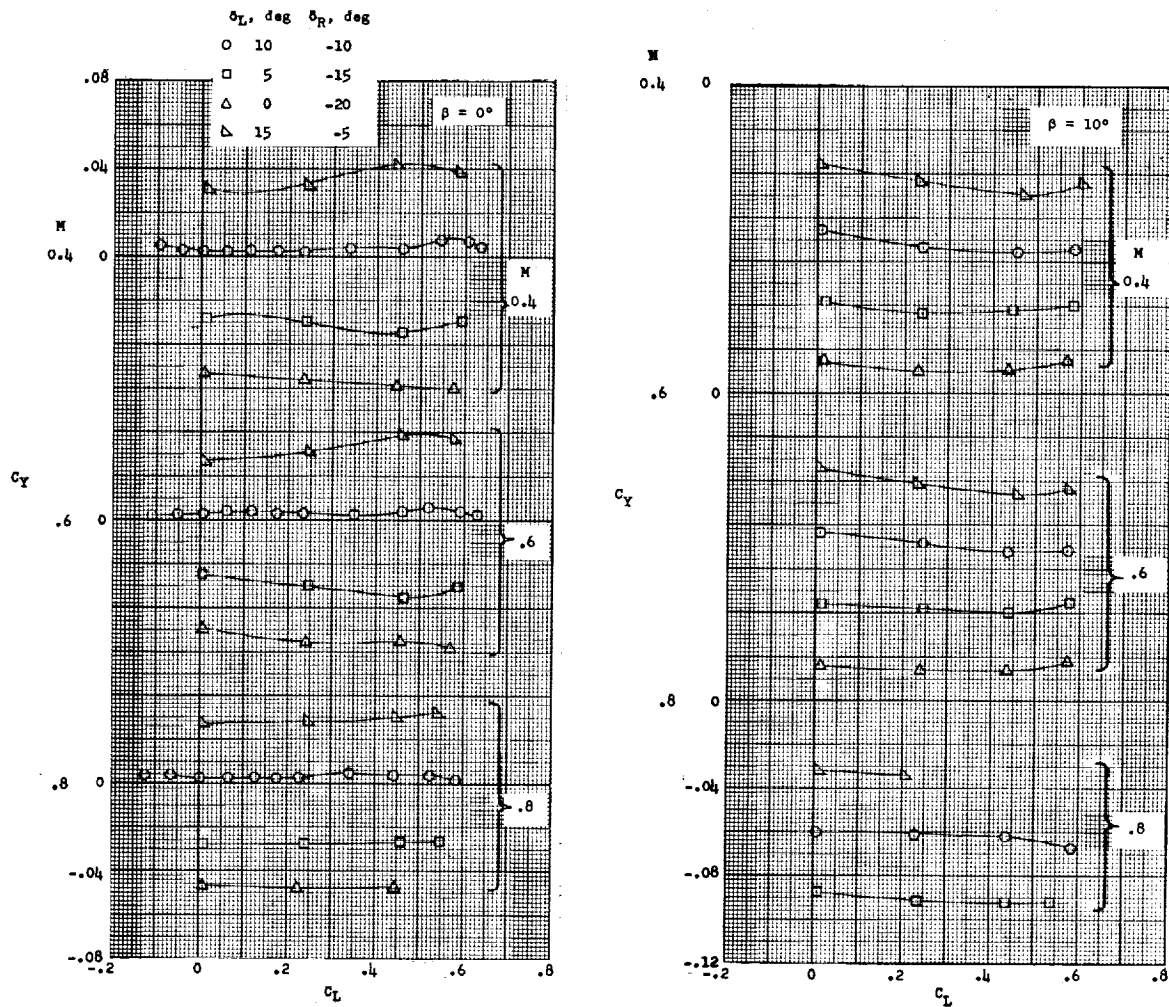
(b) Effect of nacelle yaw deflection on side-force coefficient.

Figure 12.- Continued.
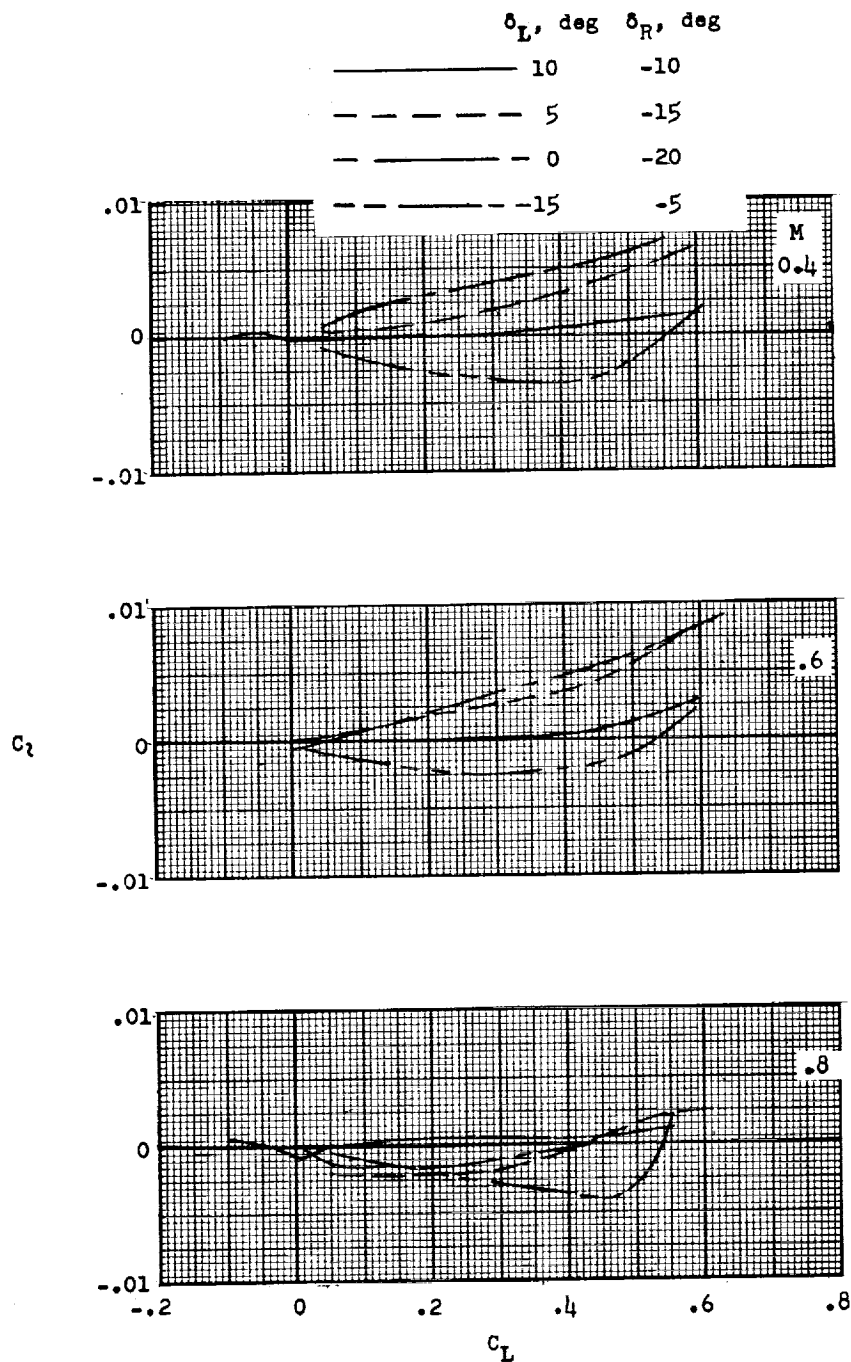
(c) Effect of nacelle yaw deflection on rolling-moment coefficient. $\beta = 0^{\circ}$.

Figure 12.- Concluded.
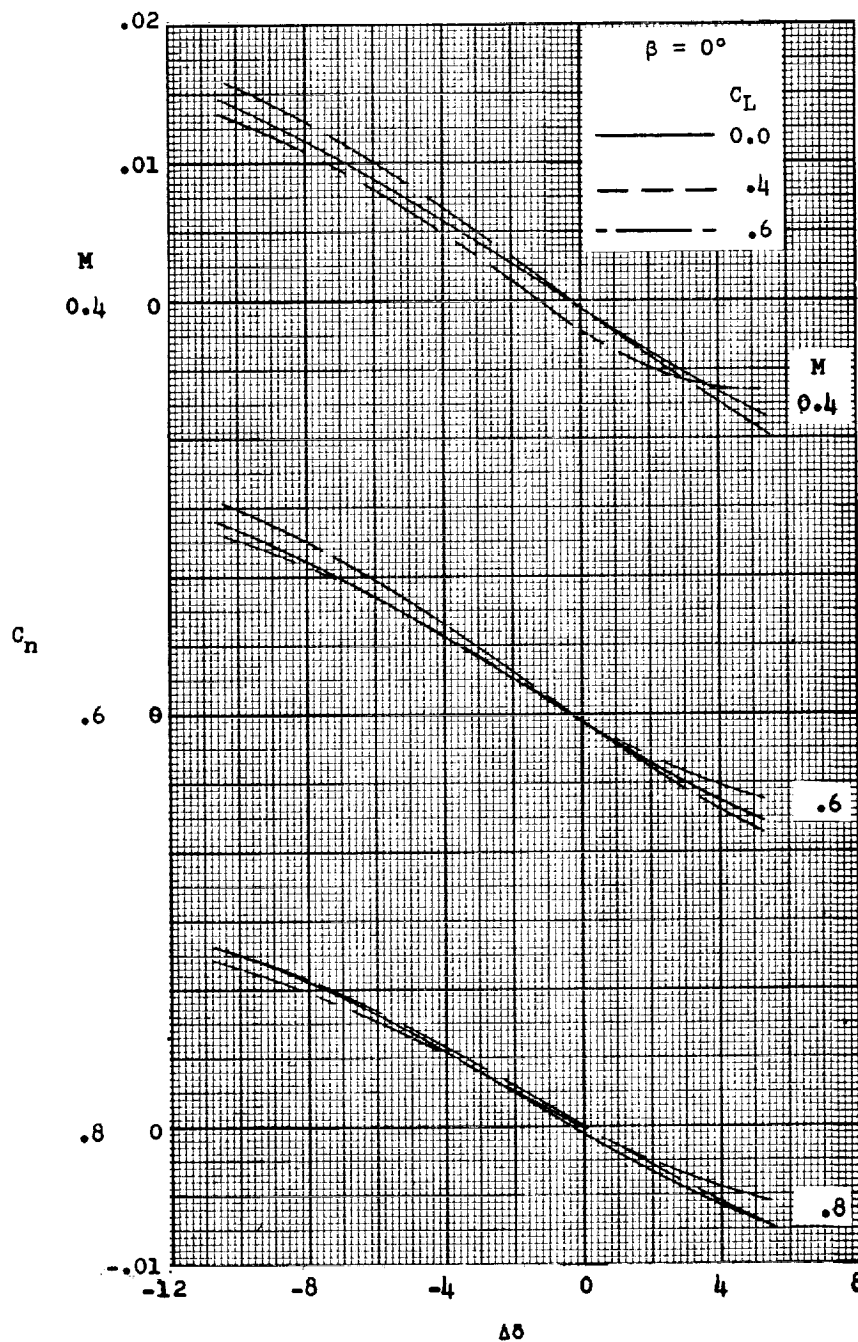
(a) Rudder effectiveness.

Figure 13.- Directional control effectiveness. Airflow nacelles with
fins; $\Lambda = 25^\circ$; $\theta_L = \theta_R = 0^\circ$; $\beta = 0^\circ$.
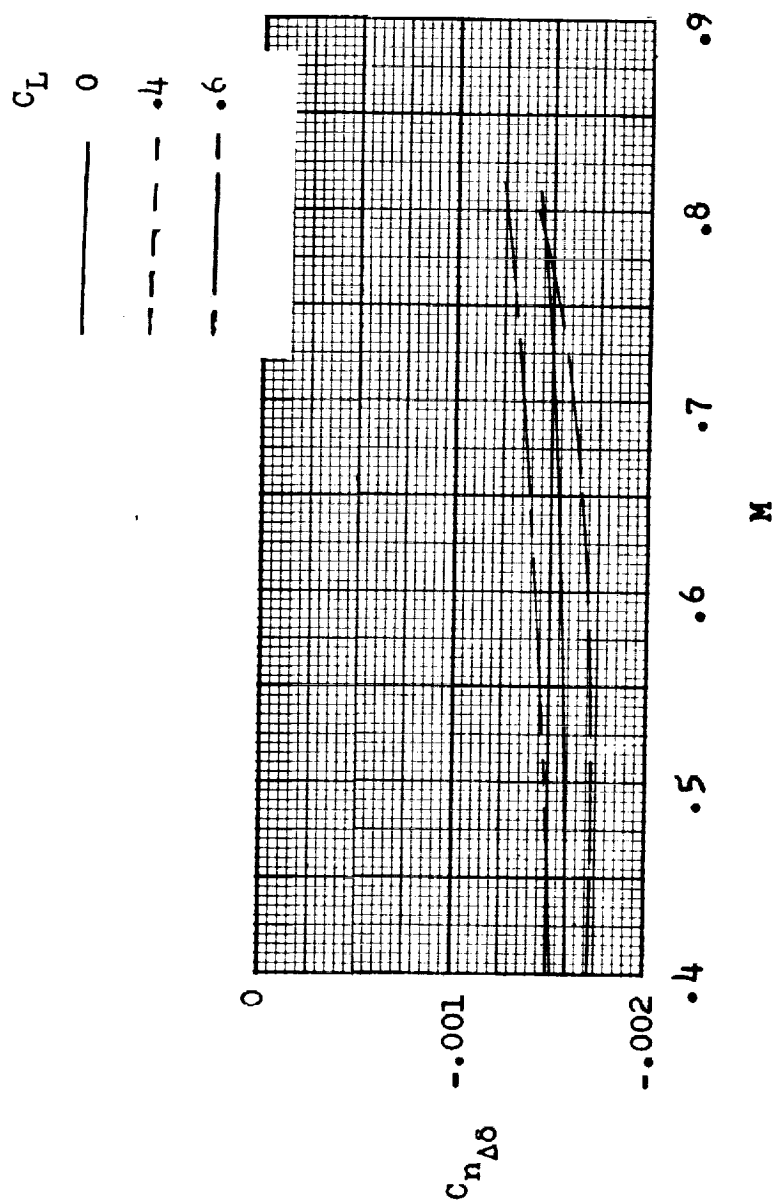
(b) Variation of $C_{n_{\Delta\delta}}$ with M.

Figure 13.- Concluded.
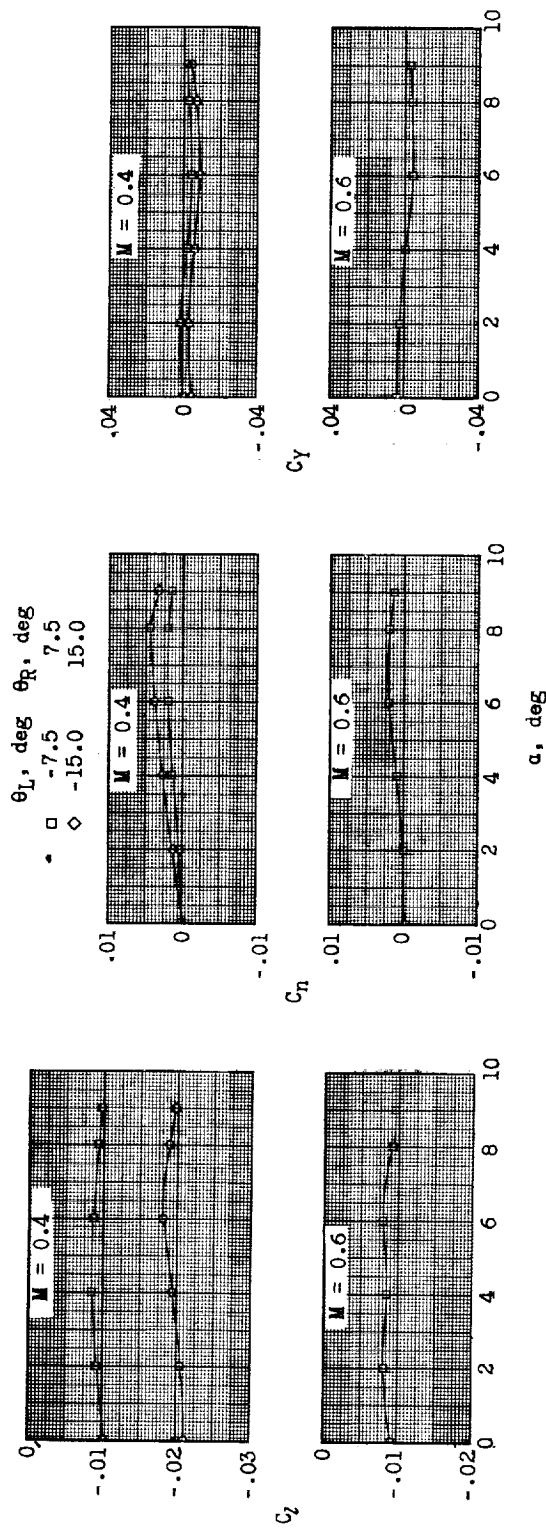
Figure 14.- Lateral control characteristics. Jet nacelles with fins; $\Lambda = 25°$; $\delta_L = 10°$; $\delta_R = -10°$; $\beta = 0°$; jets off.
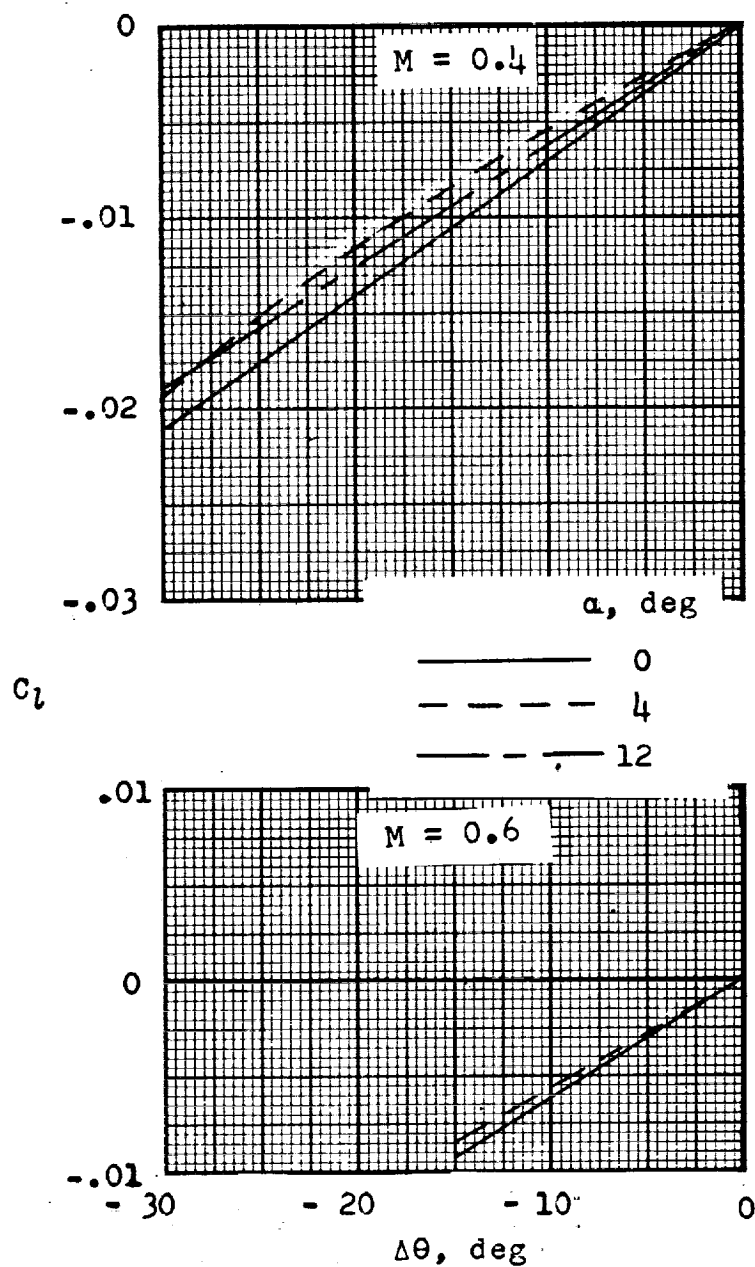
Figure 15.- Lateral control effectiveness. Jet nacelles with fins;
$\Lambda = 25°$; $\delta_L = 10°$; $\delta_R = -10°$; $\beta = 0°$; jets off.
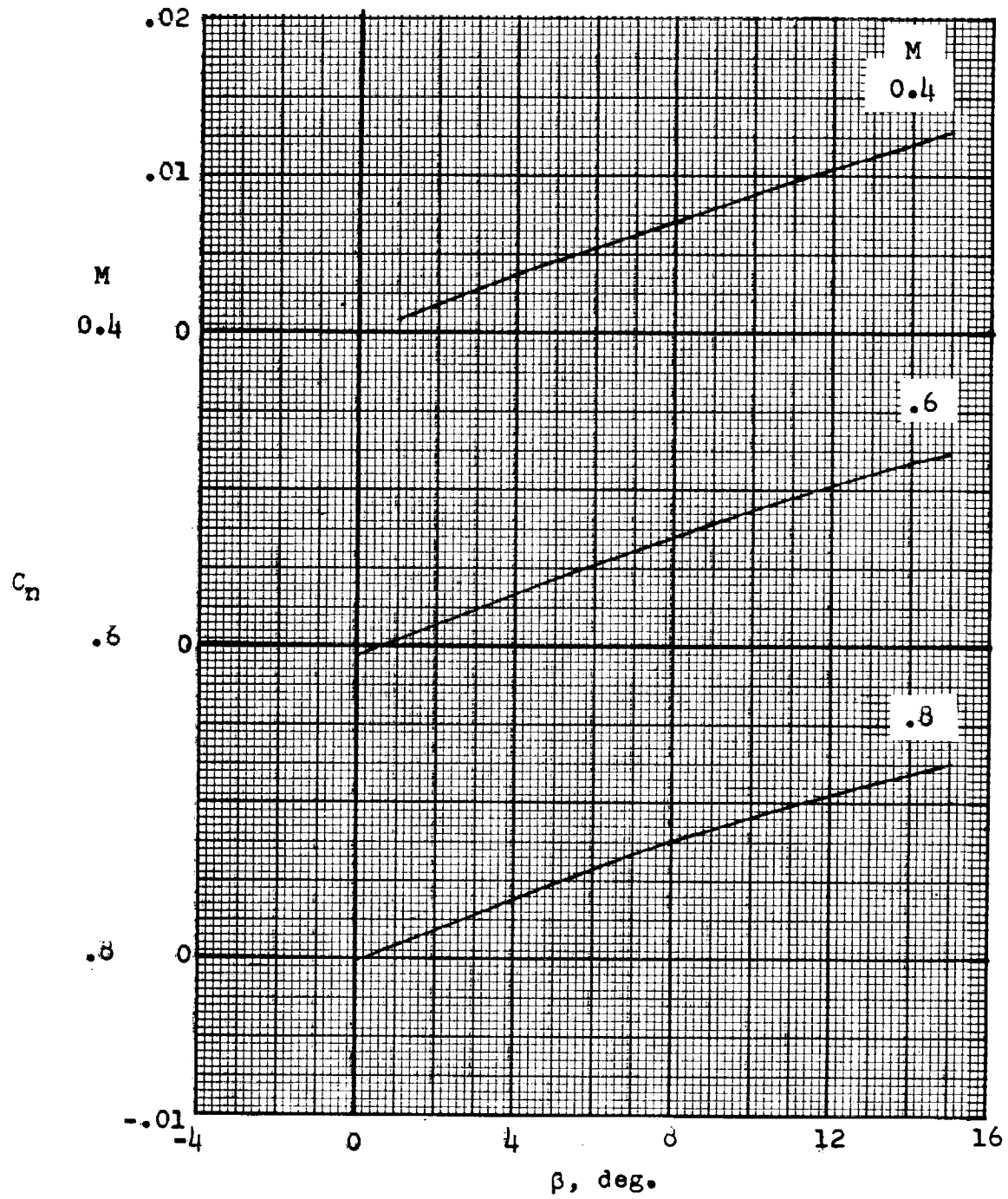
(a) Variation of C_n with β. $C_L = 0$.

Figure 16.- Directional stability characteristics.

SECRET
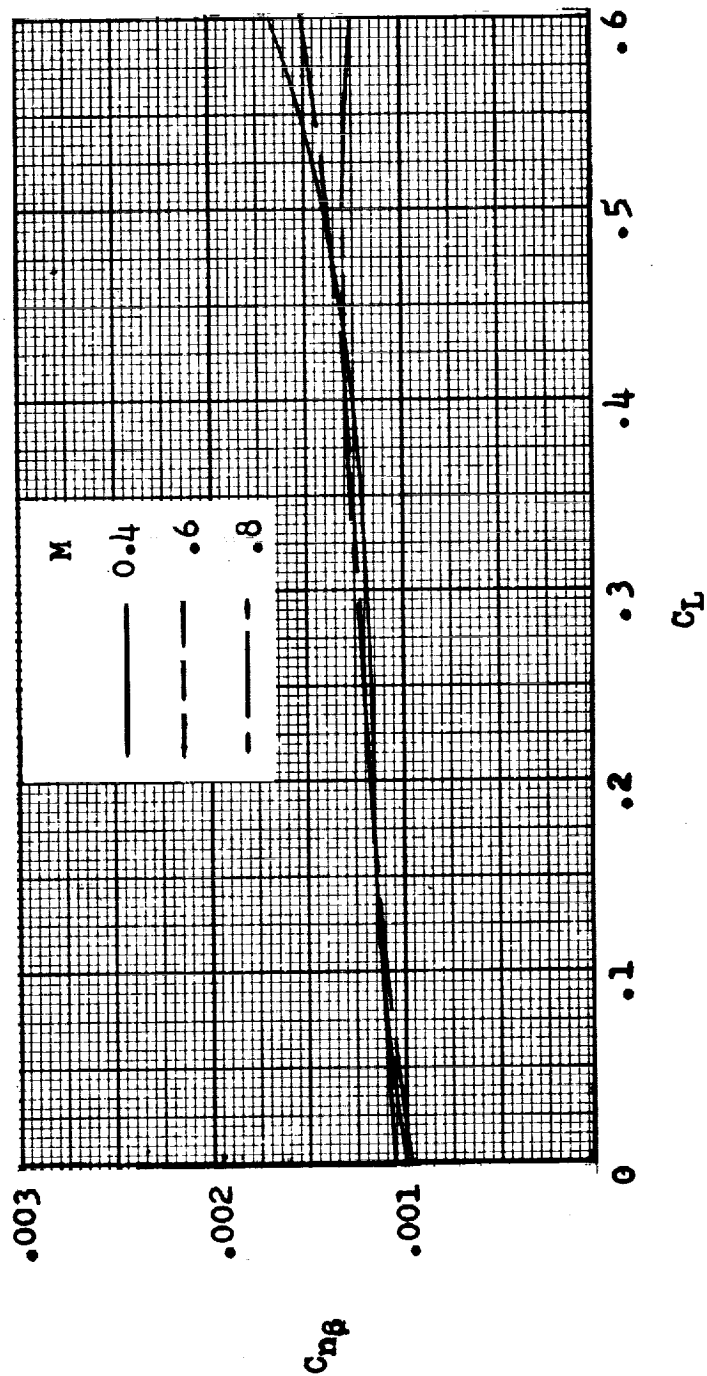
(b) Variation of C_{n_β} with C_L.

Figure 16.- Continued.
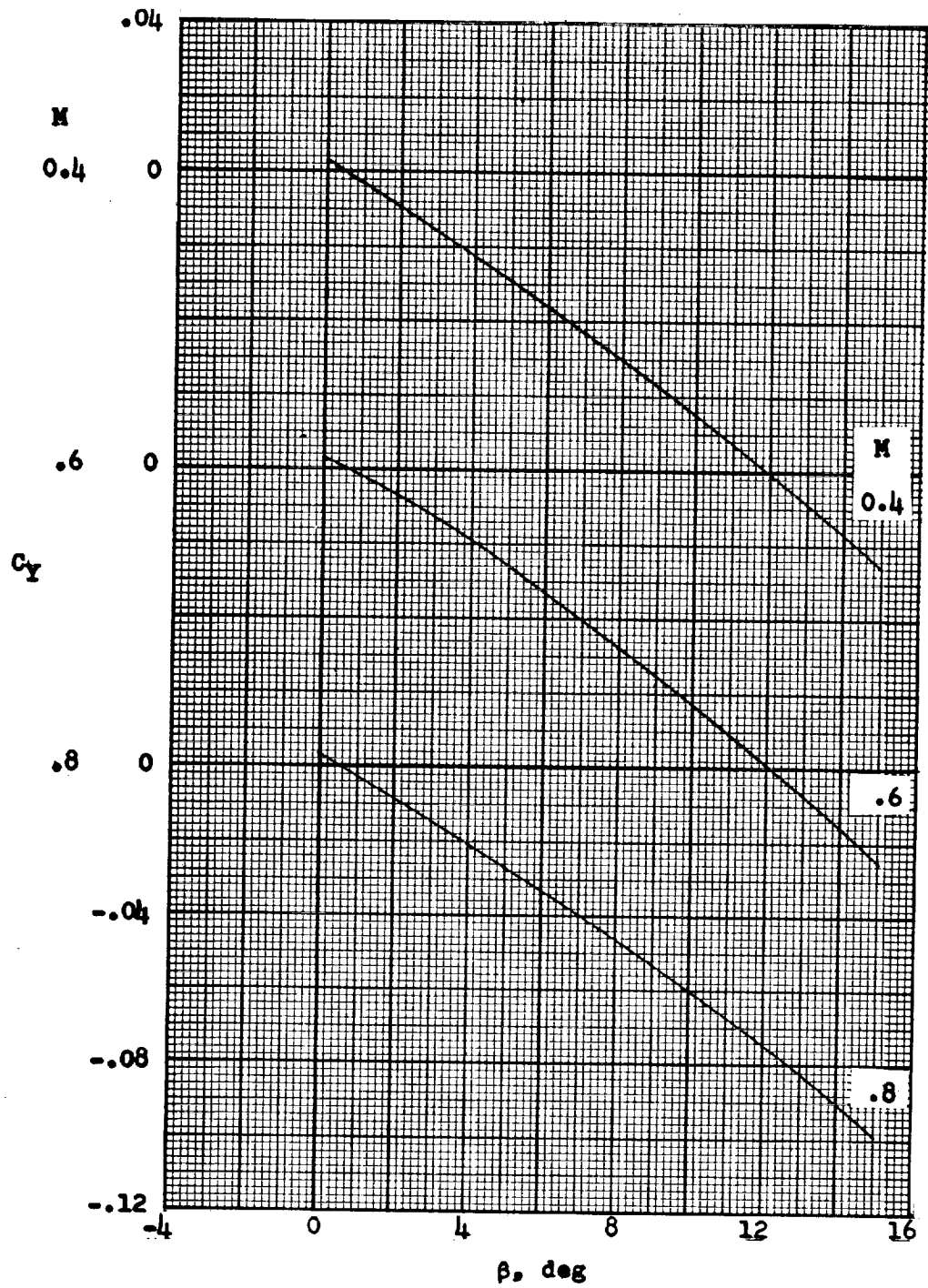
(c) Variation of C_Y with β. $C_L = 0$.

Figure 16.- Concluded.

SECRET
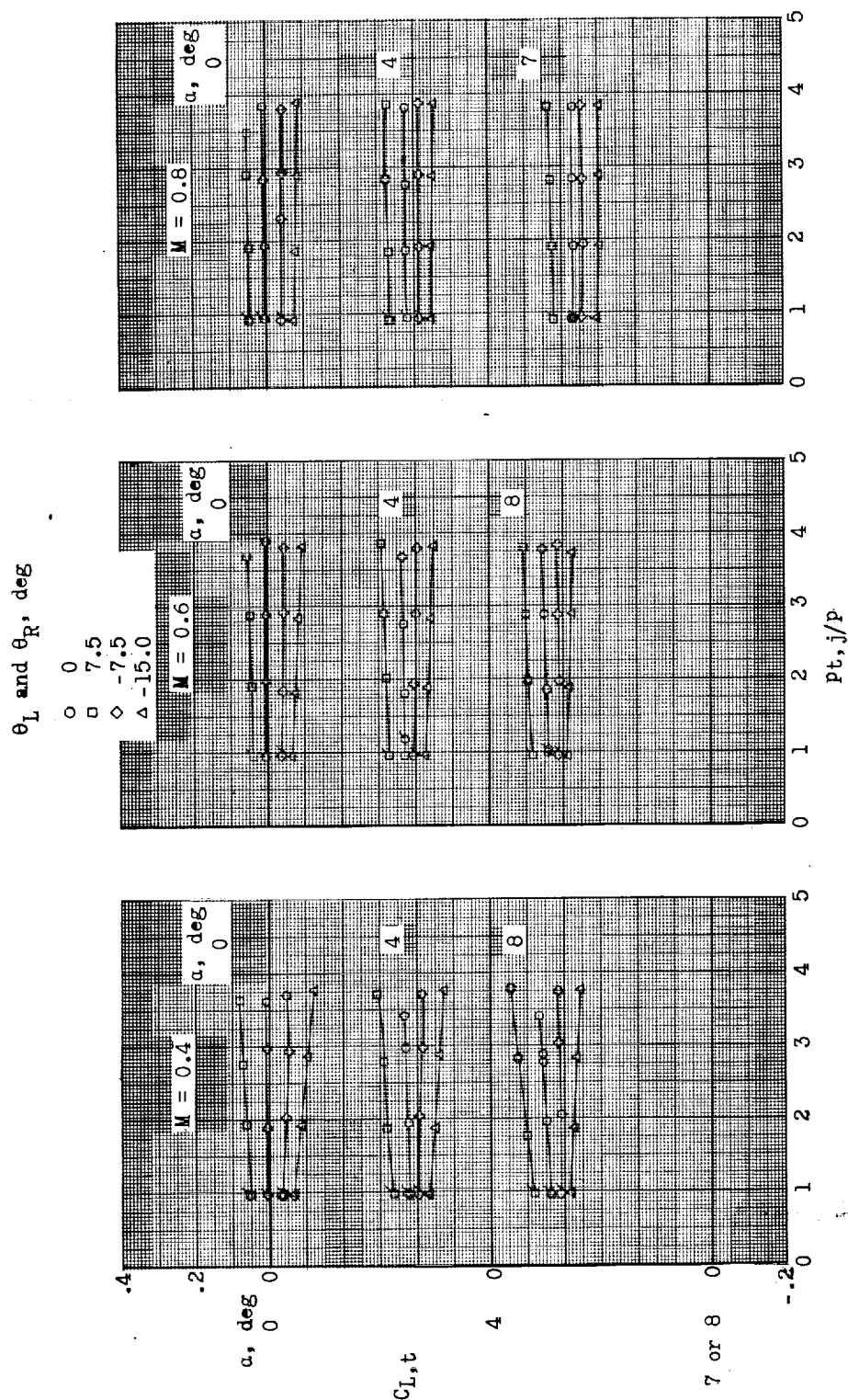
(a) Variation of lift coefficient with jet total-pressure ratio.

Figure 17.- Model forces and moments (including components of jet thrust) for several nacelle pitch deflections. Flagged symbols indicate final jets-off test points.
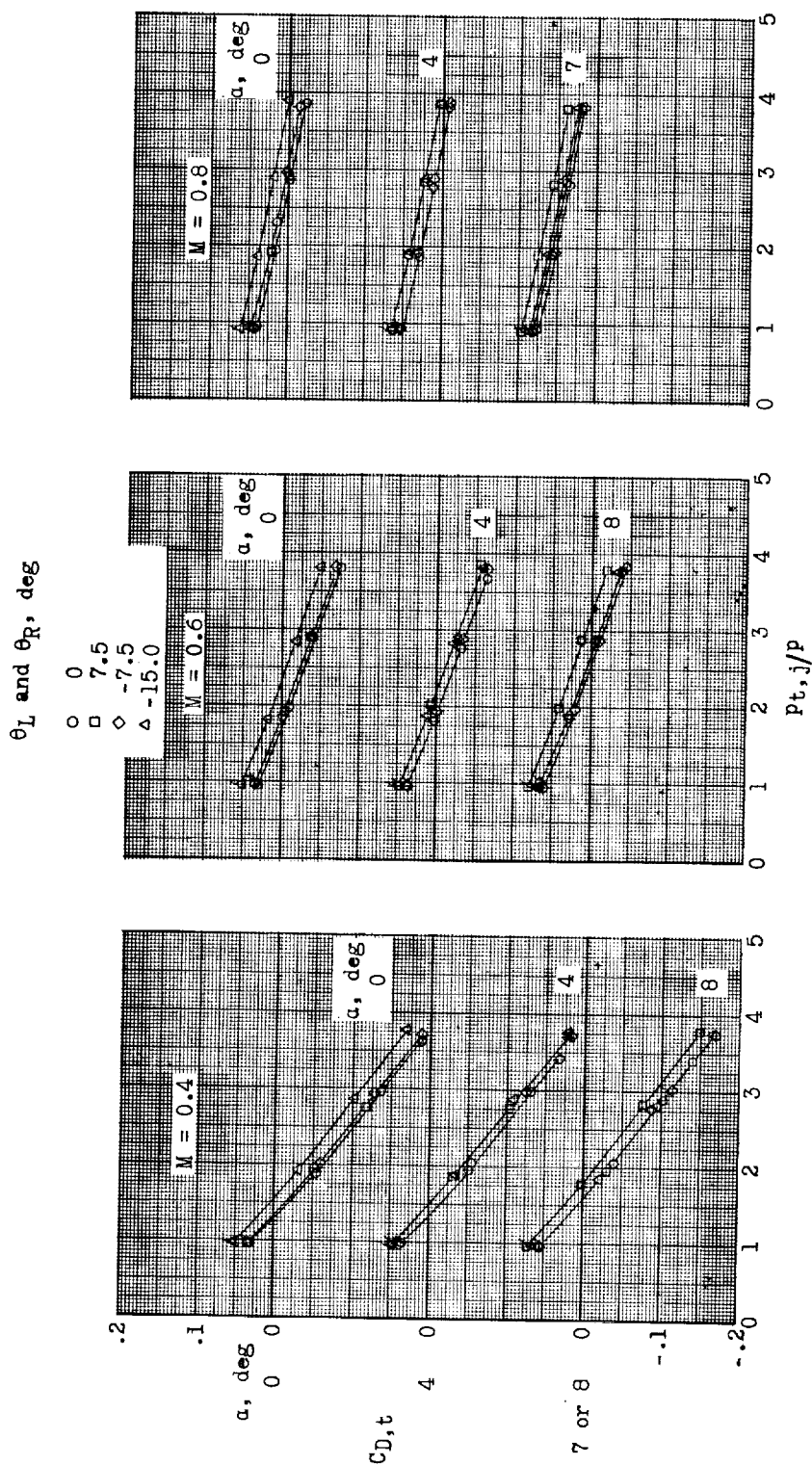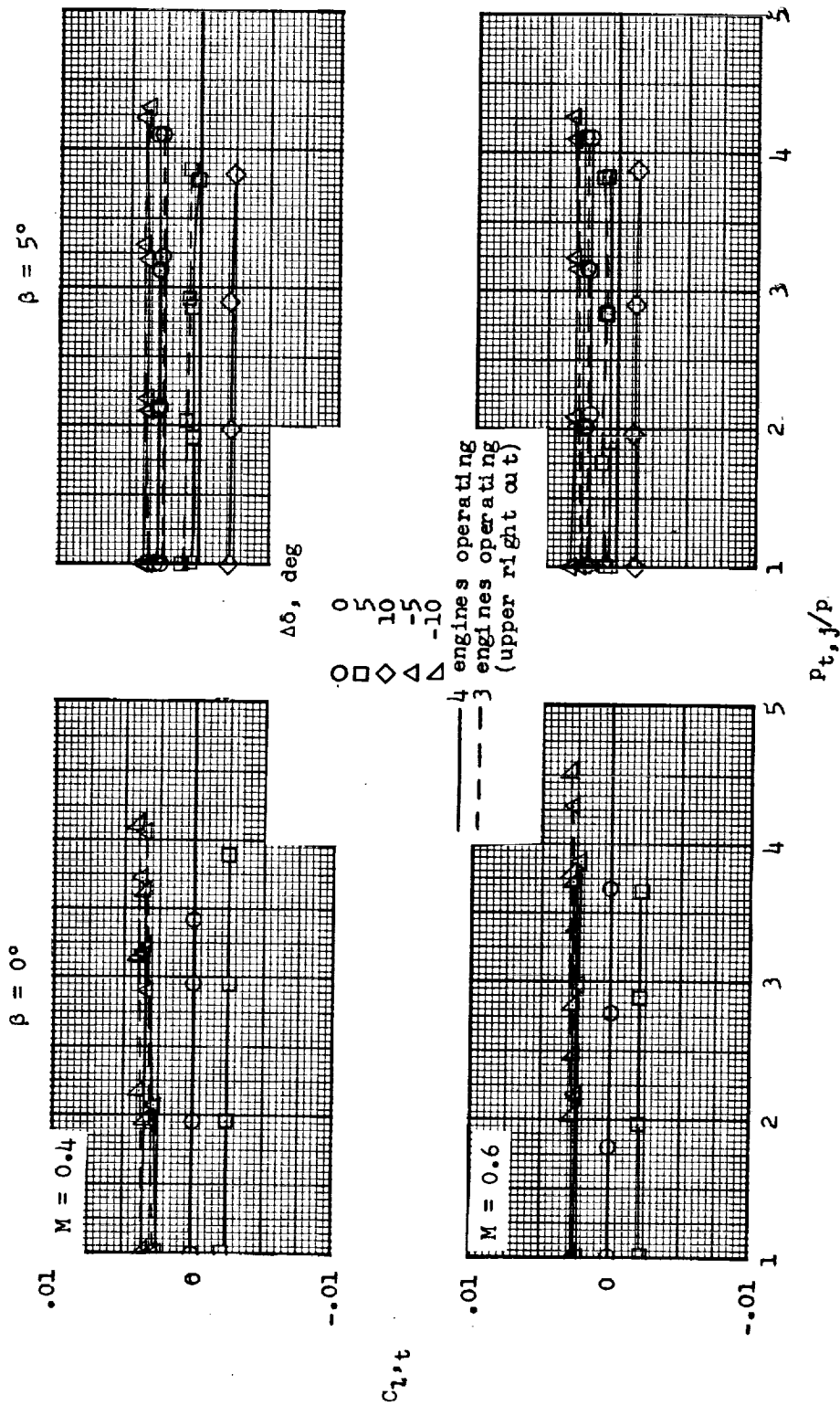
(b) Variation of drag coefficient with jet total-pressure ratio.

Figure 17.- Continued.
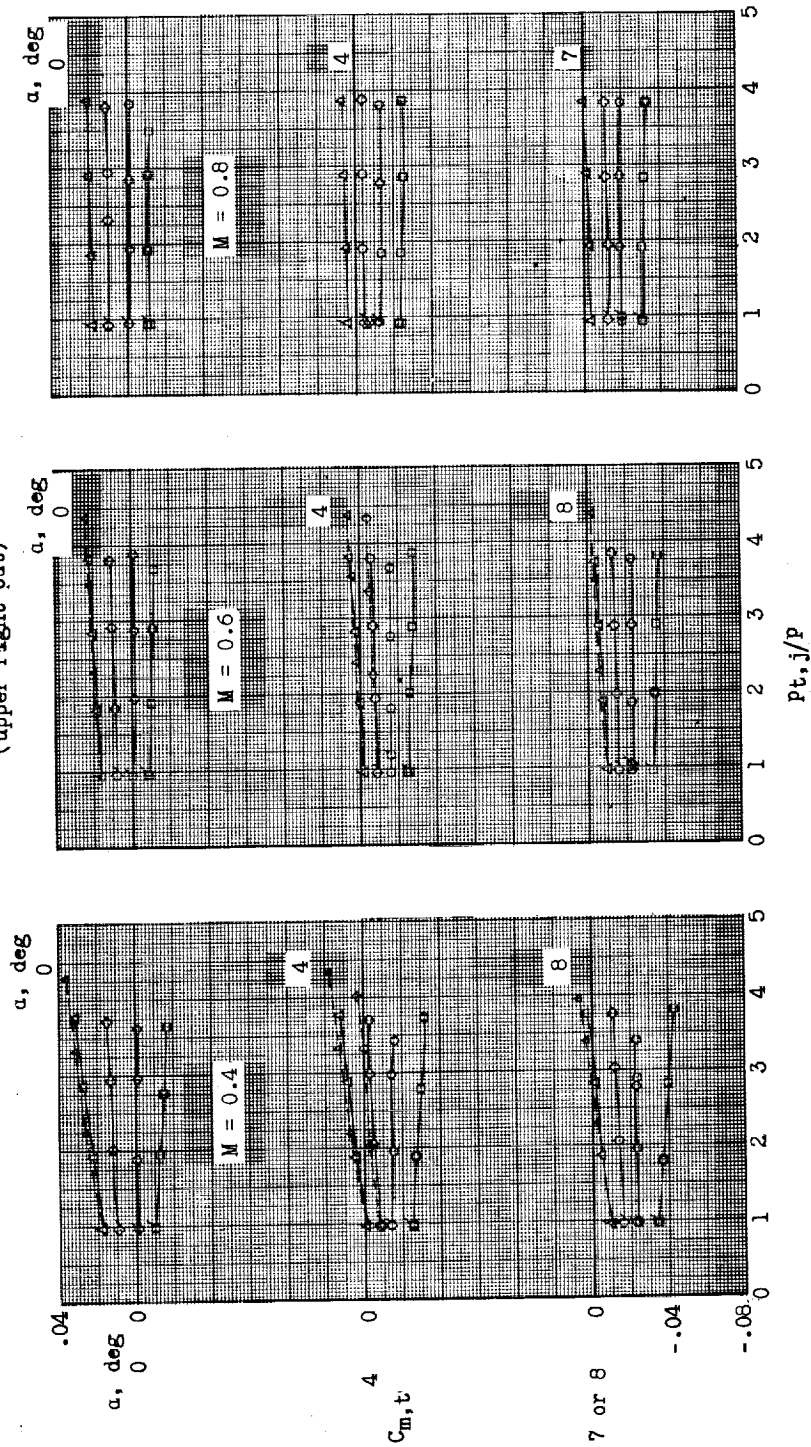
(c) Variation of pitching-moment coefficient with jet total-pressure ratio.

Figure 17.- Concluded.
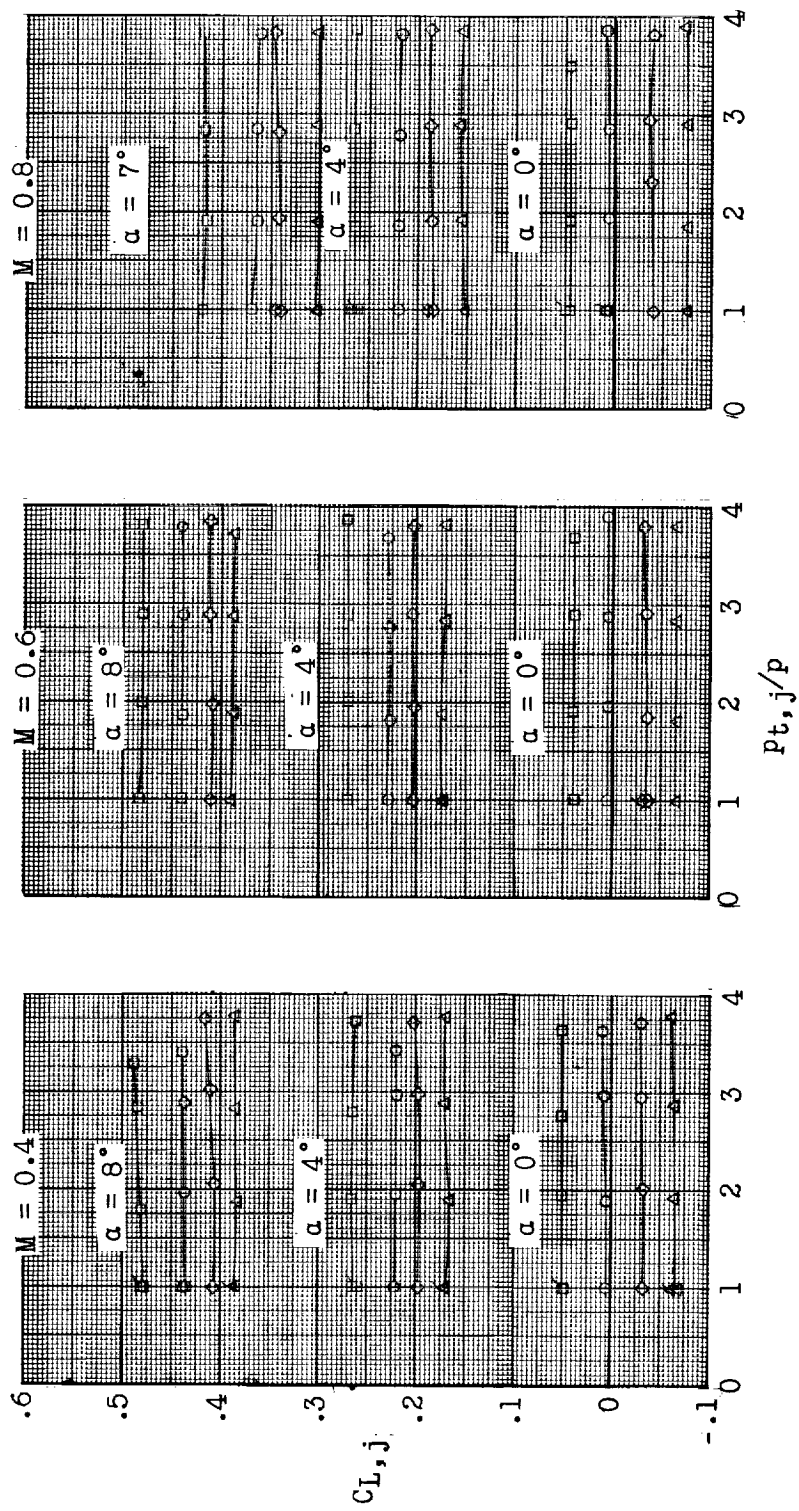
(a) Variation of lift coefficient with jet total-pressure ratio.

Figure 18.- Model forces and moments (with components of jet thrust removed) for several nacelle pitch deflections. Flagged symbols indicate final jets-off test points.
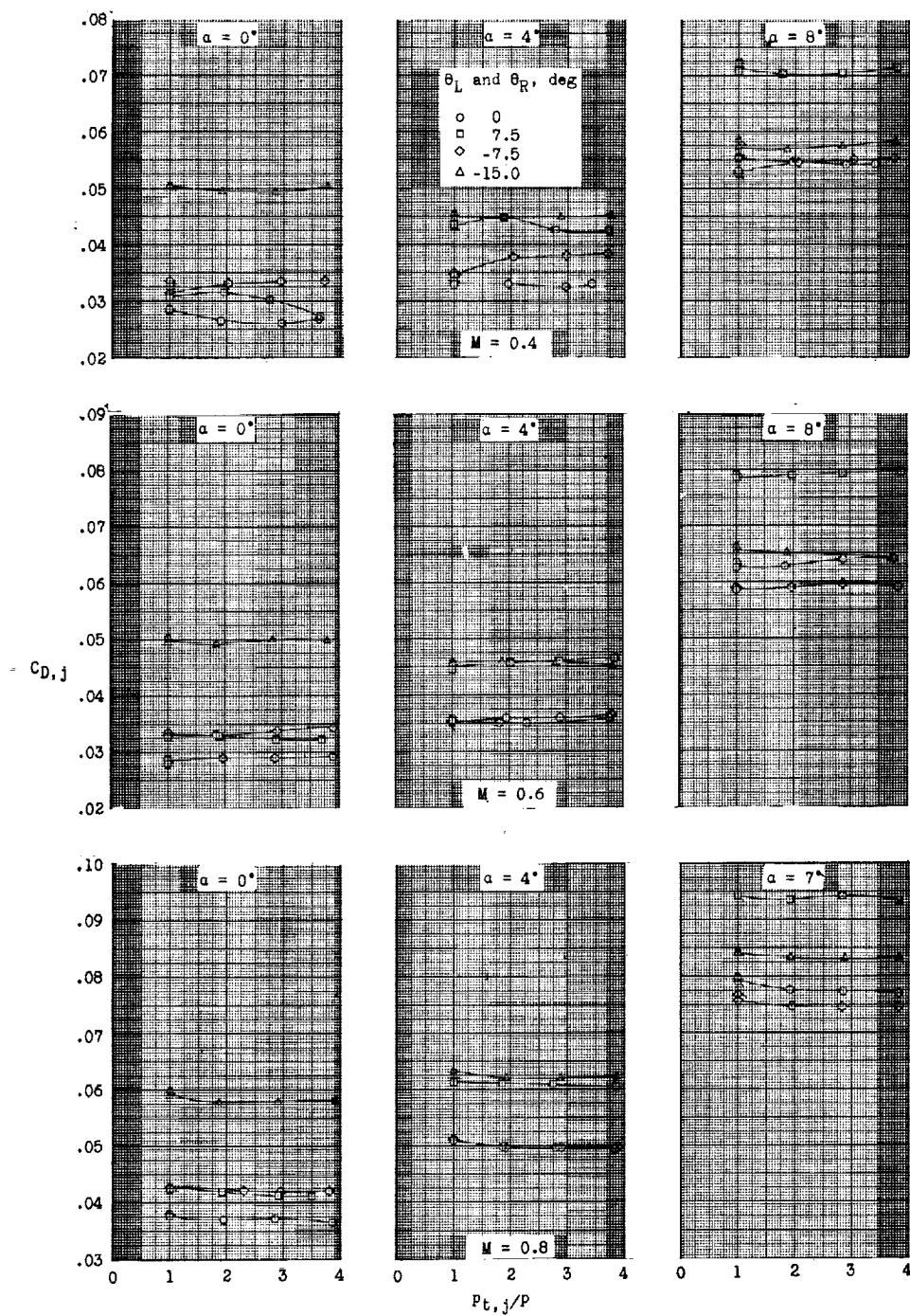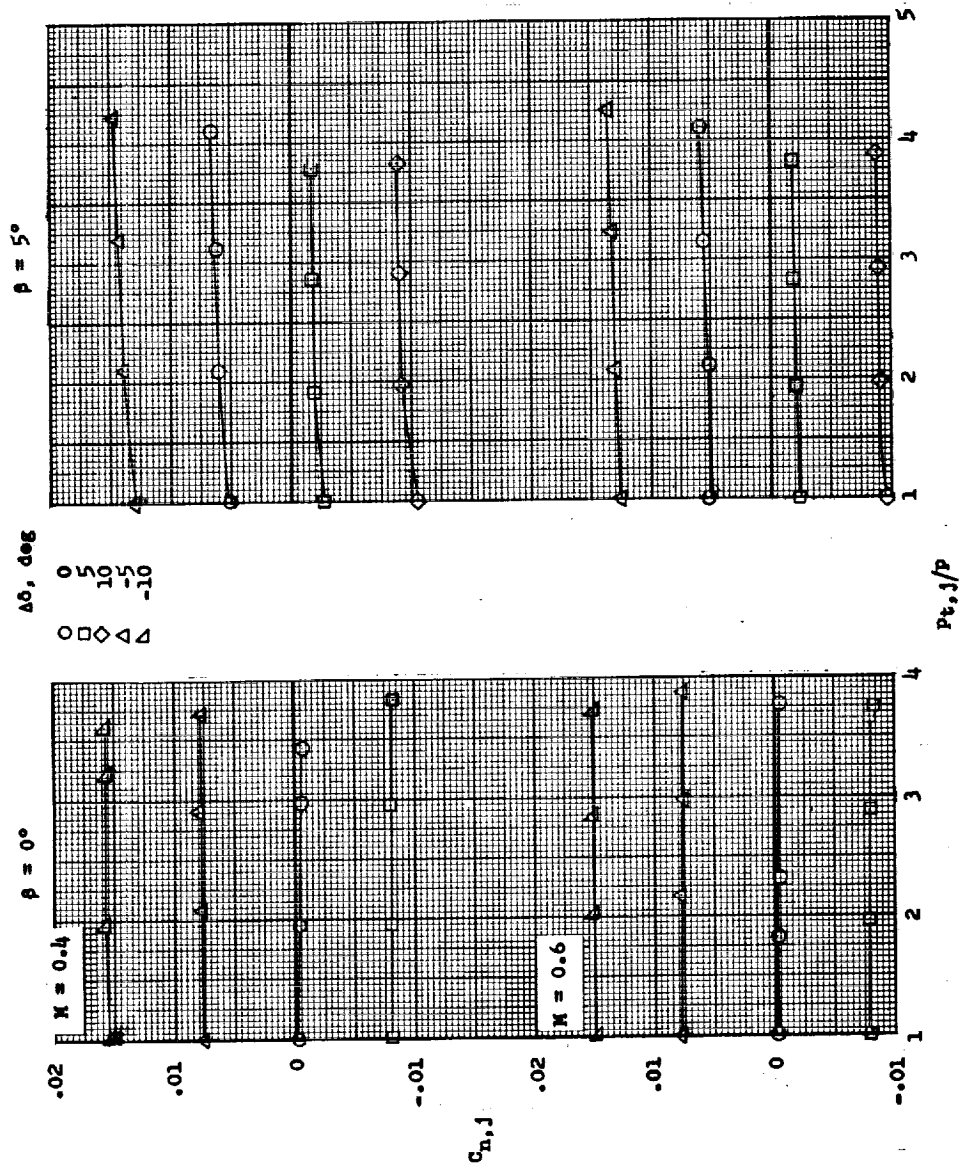
(b) Variation of drag coefficient with jet total-pressure ratio.

Figure 18.- Continued.
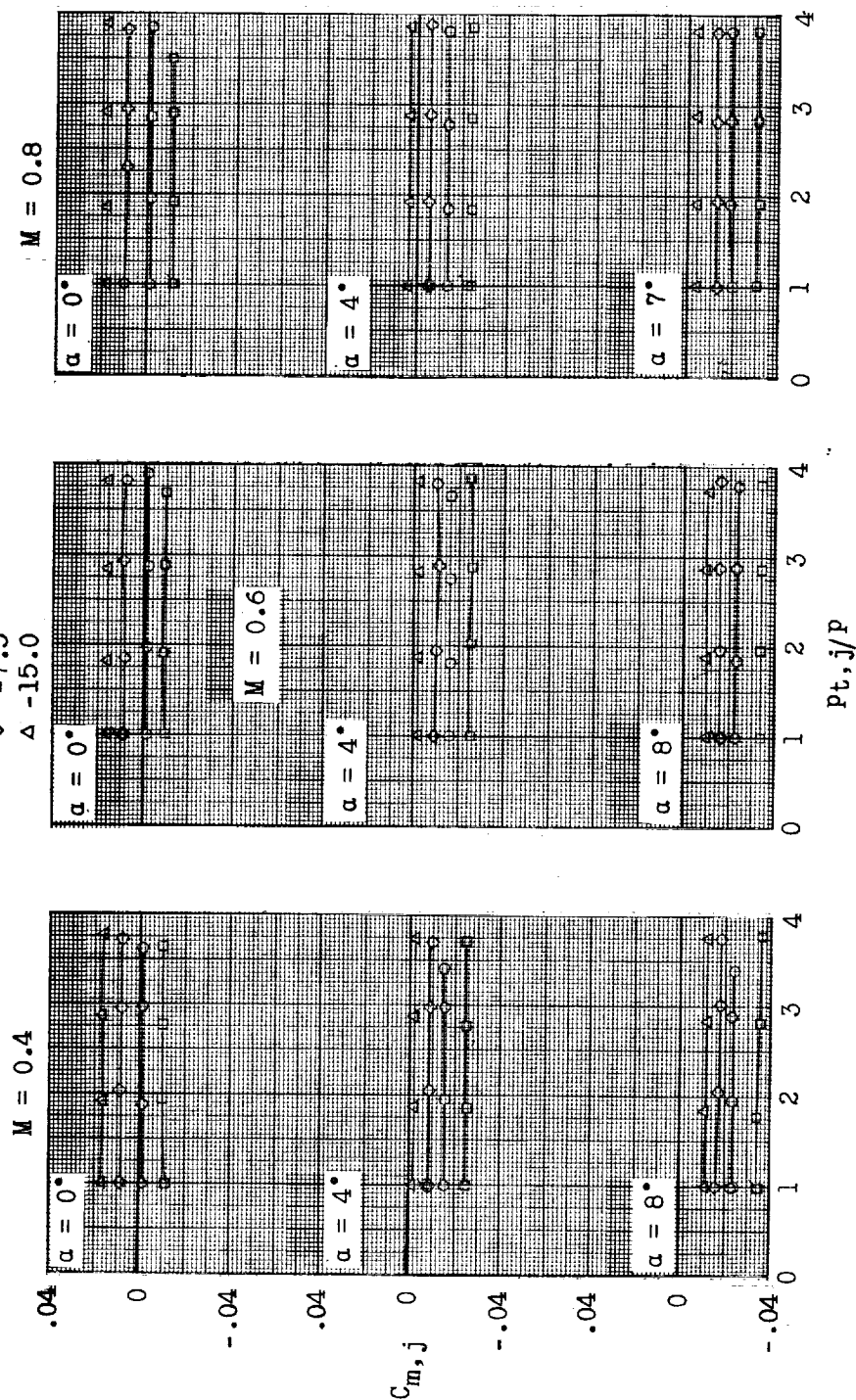
(c) Variation of pitching-moment coefficient with jet total-pressure ratio.

Figure 18.- Concluded.
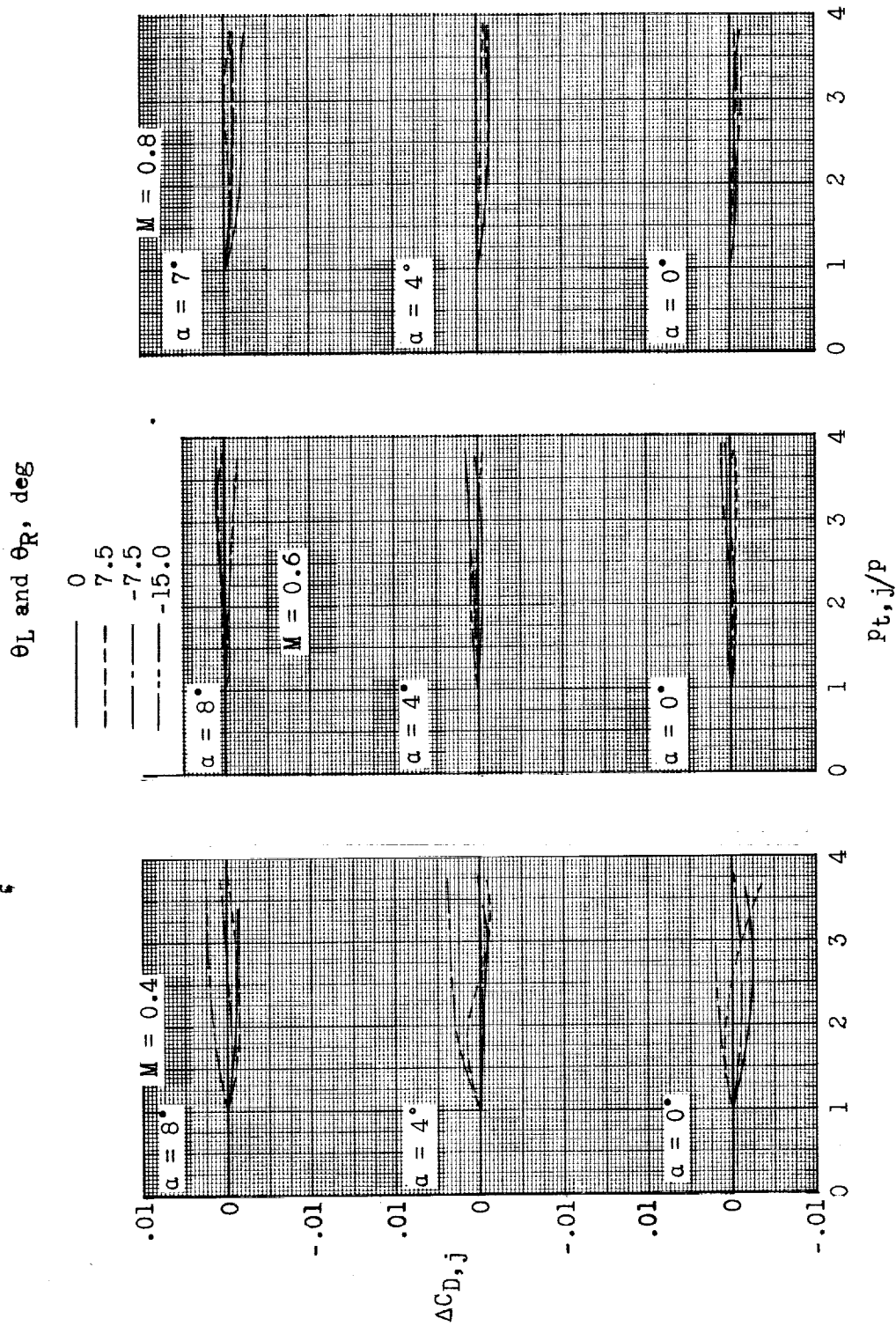
Figure 19.- Variation of incremental drag coefficient with jet total-pressure ratio.
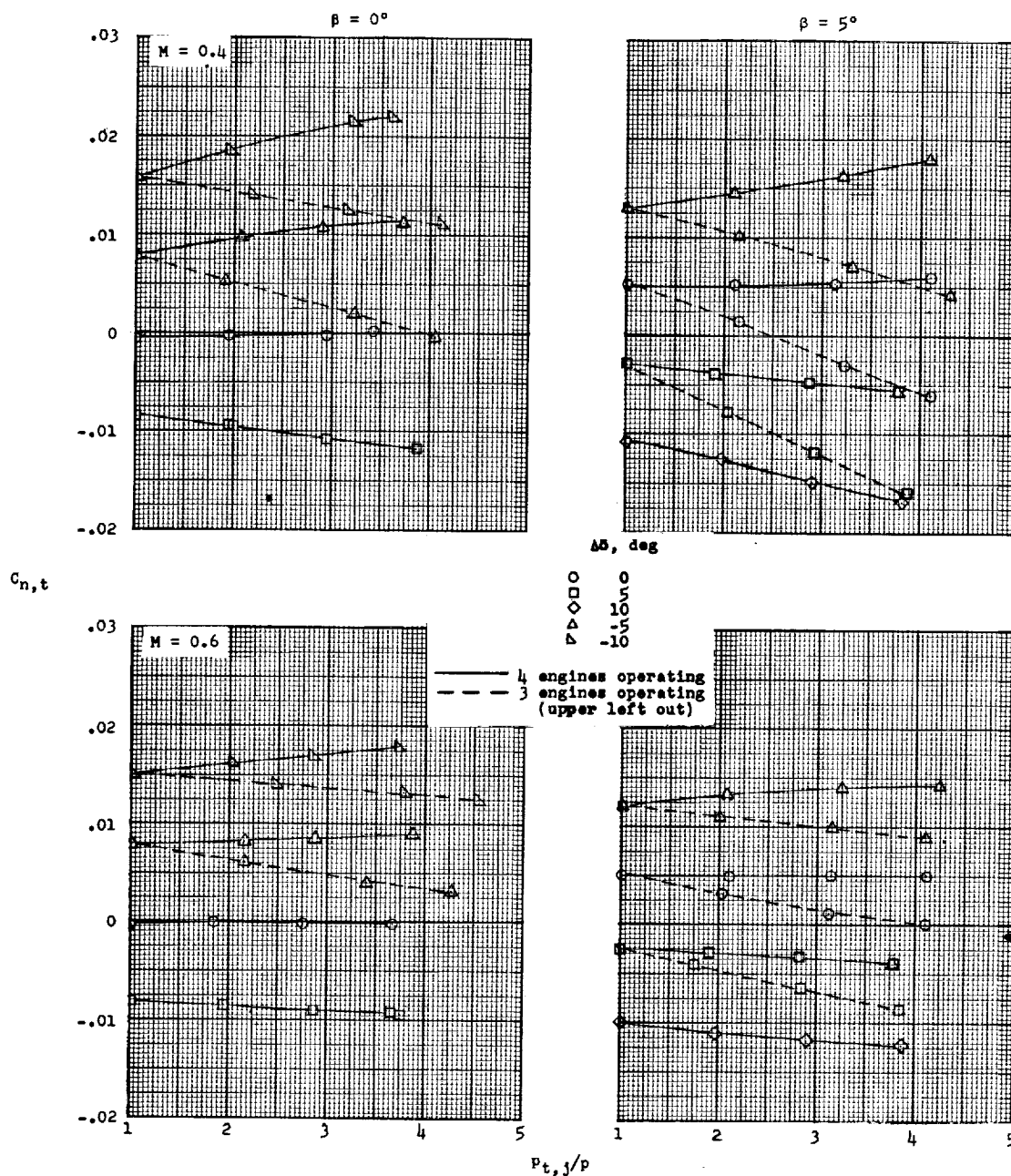
(a) Variation of yawing-moment coefficient with jet total-pressure ratio.

Figure 20.- Model forces and moments (including components of jet thrust) for several nacelle yaw deflections and for sideslip angles of $0°$ and $5°$. $\alpha = 4°$.
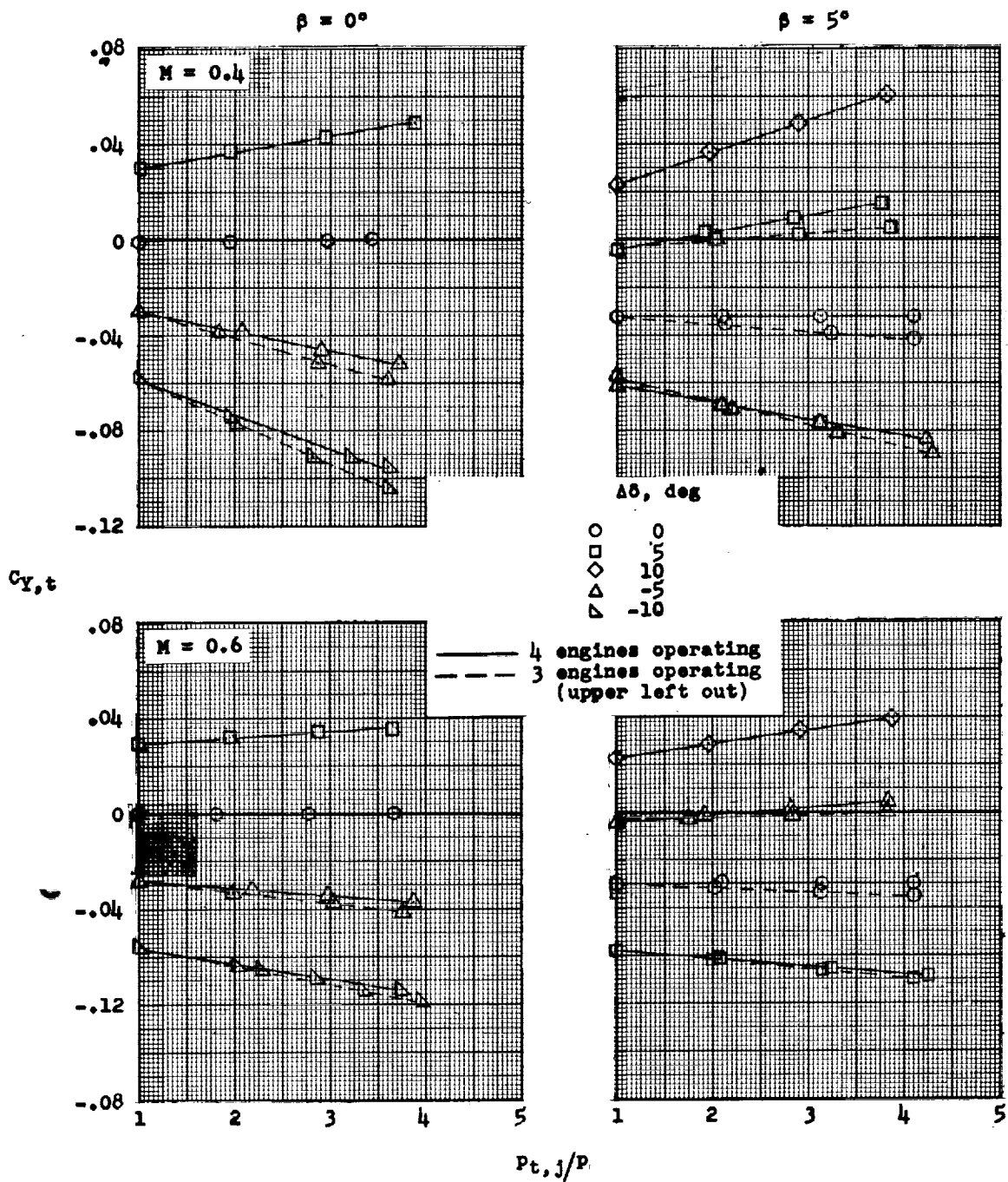
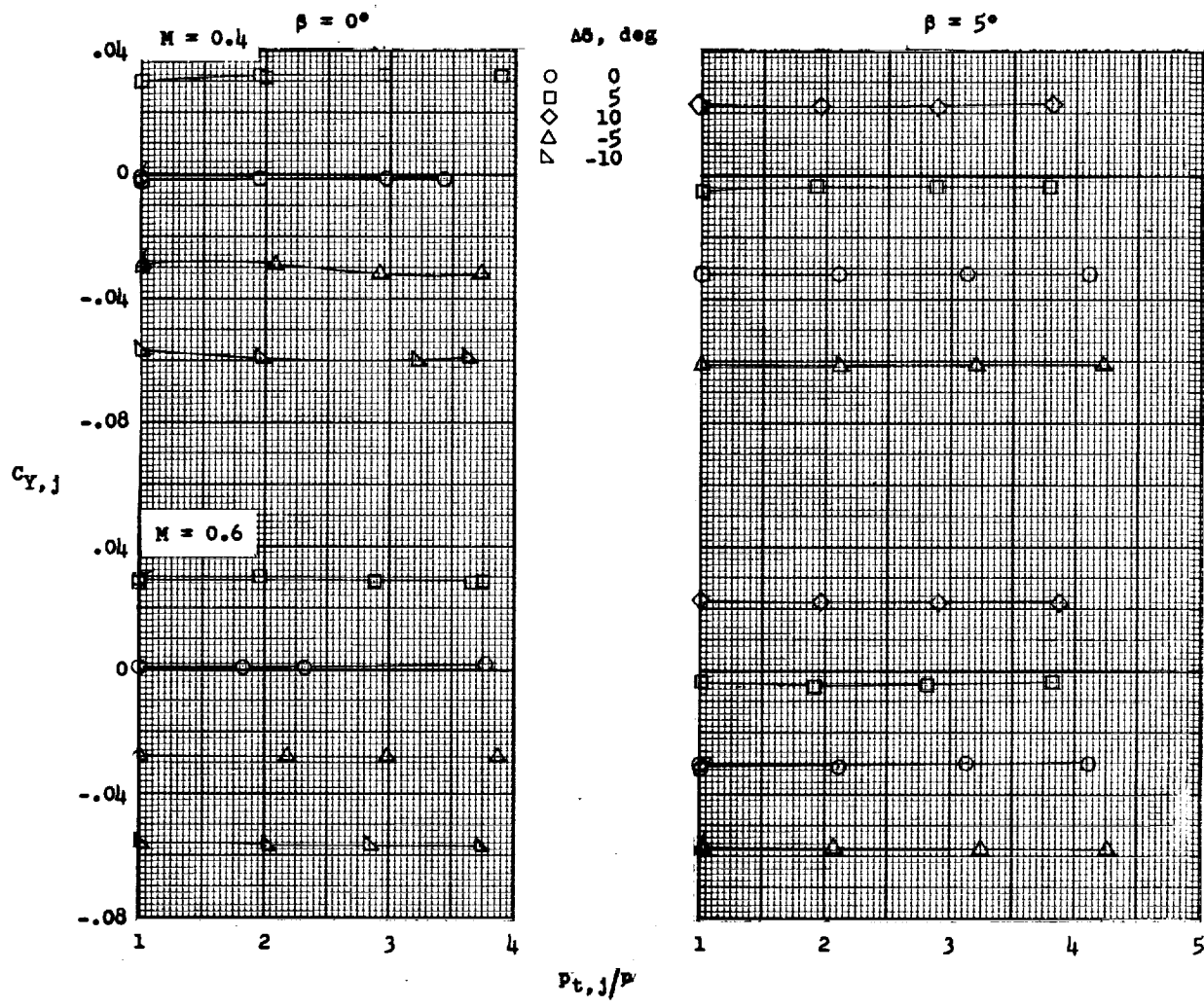(b) Variation of side-force coefficient with jet total-pressure ratio.

Figure 20.- Continued.

(c) Variation of rolling-moment coefficient with jet total-pressure ratio.
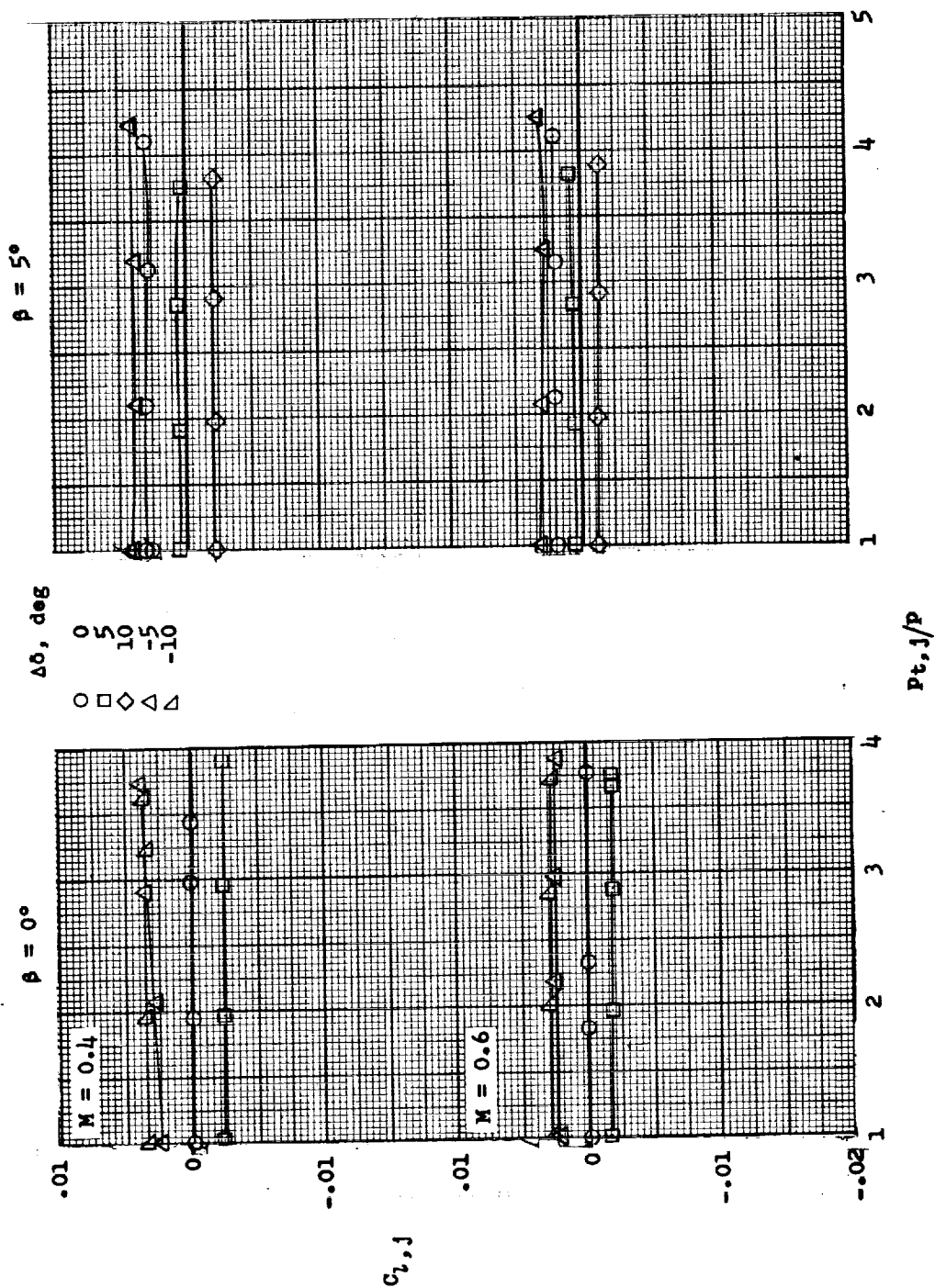
Figure 20.- Concluded.

(a) Variation of yawing-moment coefficient with jet total-pressure ratio.

Figure 21.- Model forces and moments (with components of jet thrust removed) for several nacelle yaw deflections and for sideslip angles of 0° and 5°. $\alpha = 4^\circ$.
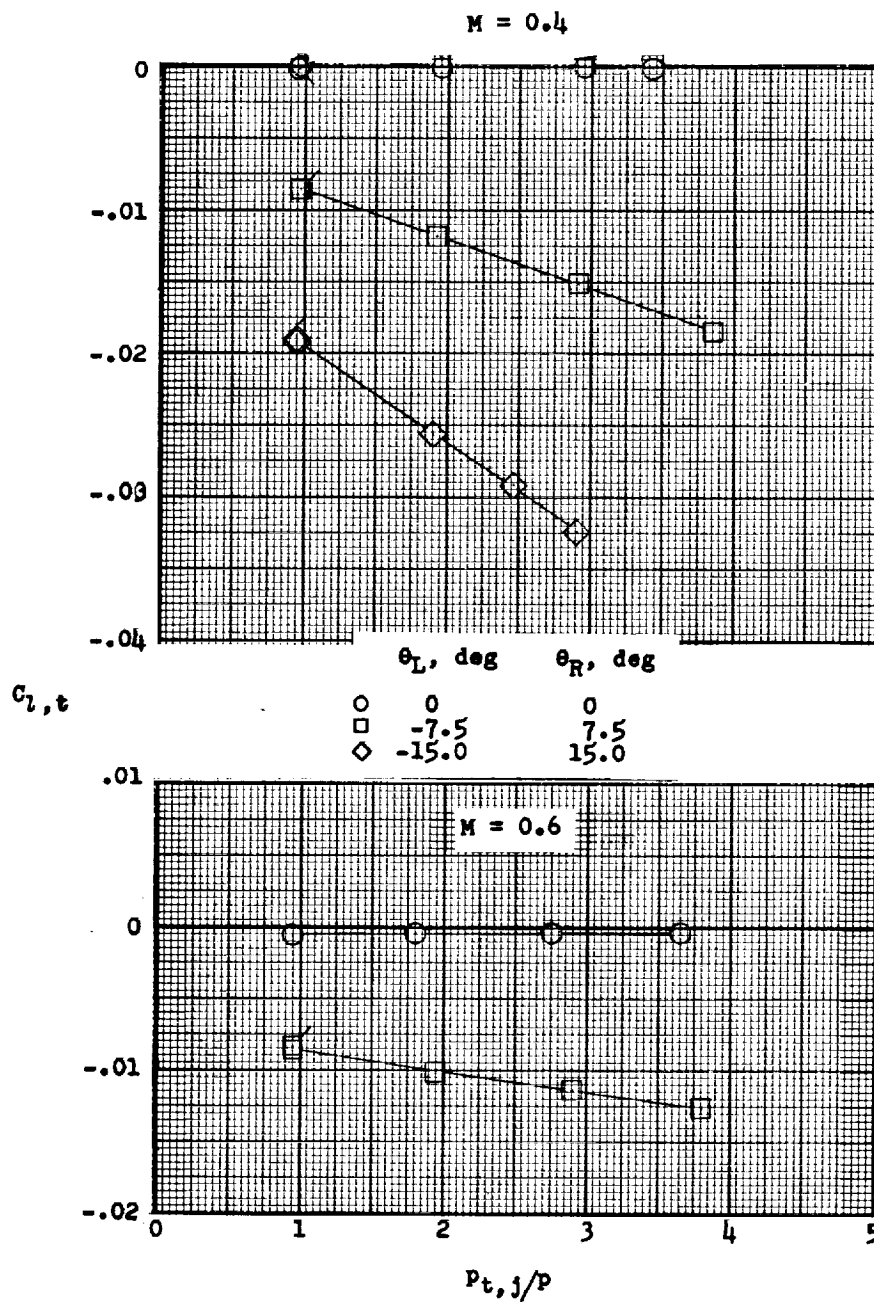
(b) Variation of side-force coefficient with jet total-pressure ratio.

Figure 21.- Continued.

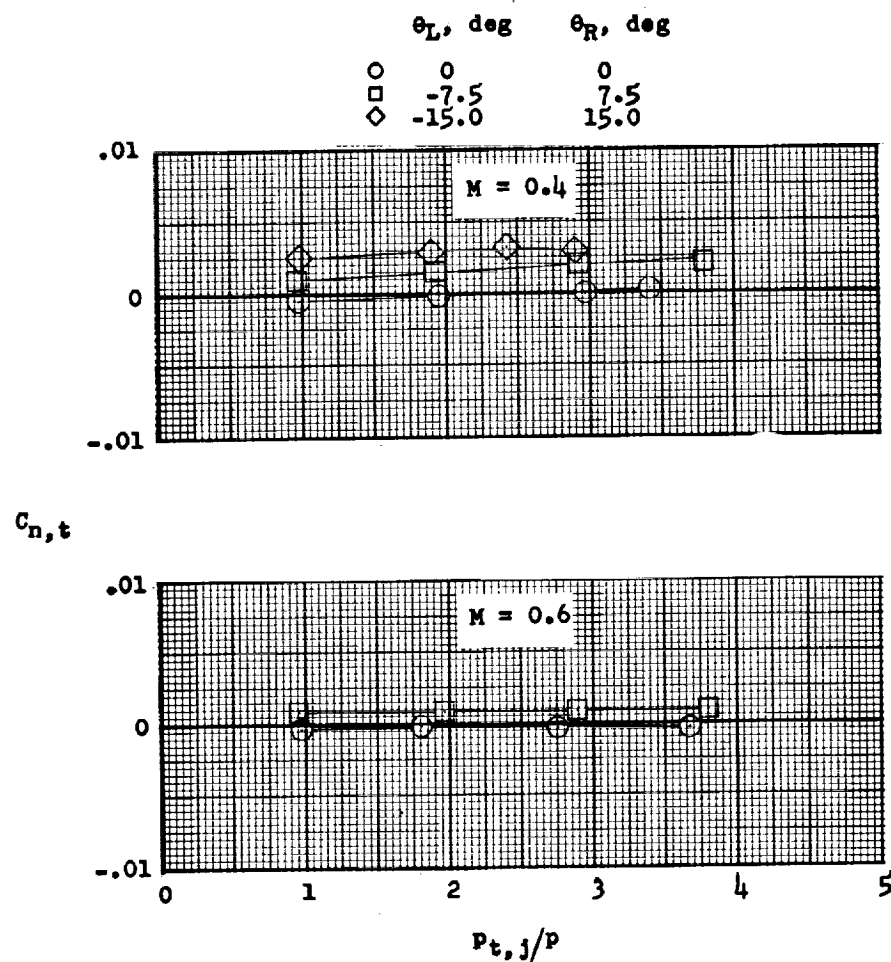(c) Variation of rolling-moment coefficient with jet total-pressure ratio.

Figure 21.- Concluded.

M = 0.4

θ_L, deg	θ_R, deg
O 0	0
□ -7.5	7.5
◇ -15.0	15.0

M = 0.6

$C_{l,t}$

$p_{t,j}/p$

(a) Variation of rolling-moment coefficient (including components of jet thrust) with jet total-pressure ratio.
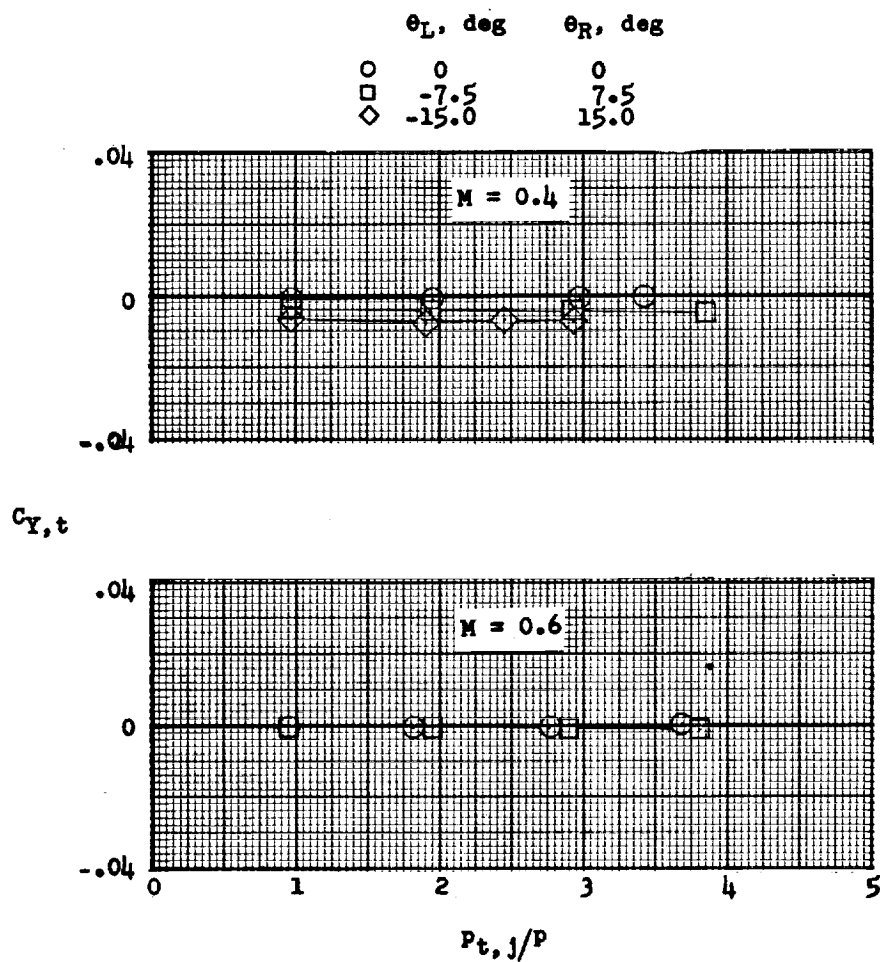
Figure 22.- Effect of jet operation on model forces and moments for several nacelle differential deflections in the pitch plane. $\alpha = 4^\circ$.

(b) Variation of yawing-moment coefficient (including components of jet thrust) with jet total-pressure ratio.

Figure 22.- Continued.

	θ_L, deg	θ_R, deg
○	0	0
□	-7.5	7.5
◇	-15.0	15.0

$$M = 0.4$$

$$M = 0.6$$

$C_{Y,t}$

$P_{t,j}/P$

(c) Variation of side-force coefficient (including component of jet thrust) with jet total-pressure ratio.
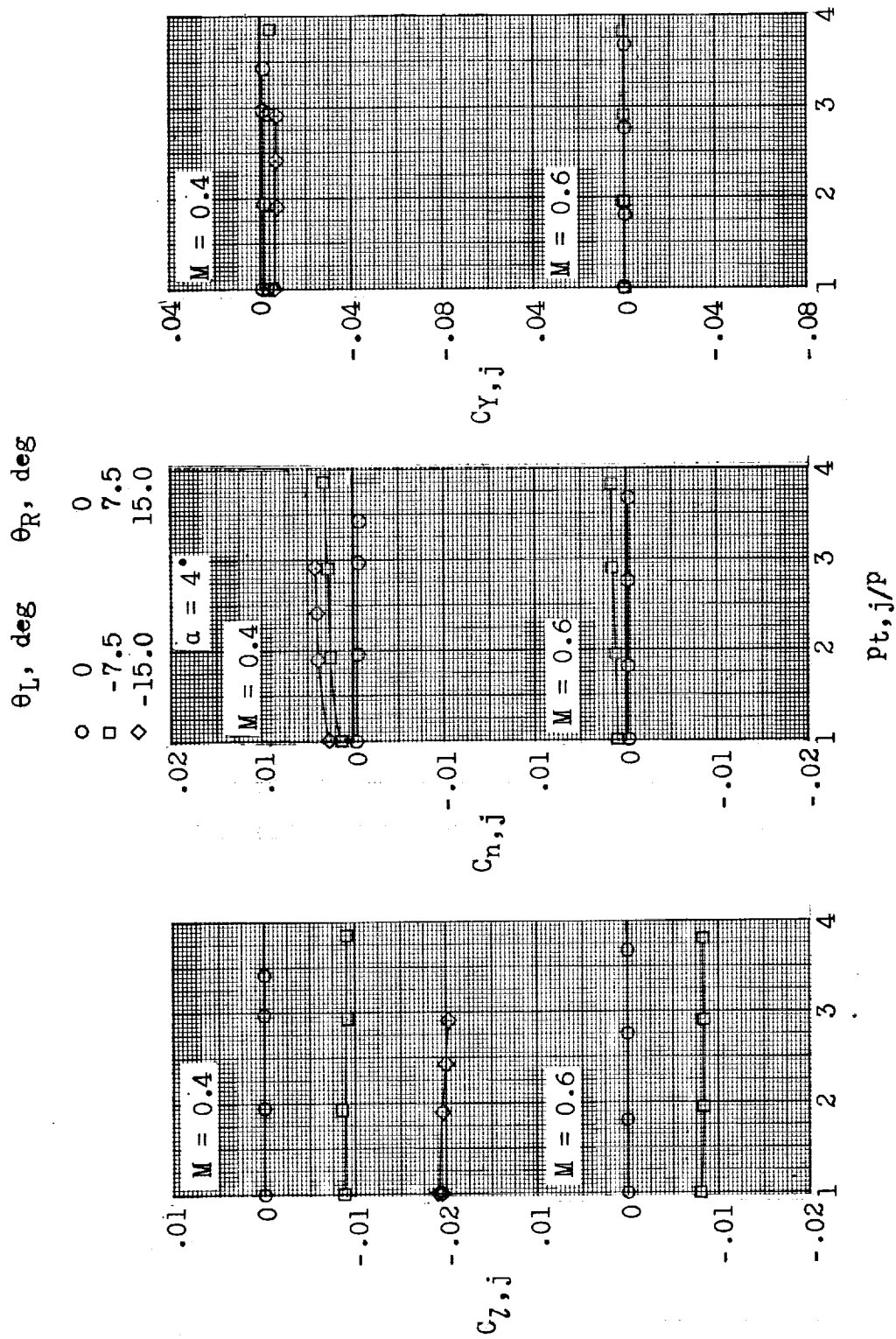
Figure 22.- Concluded.

Figure 23.- Model forces and moments (with components of jet thrust removed) for several nacelle differential deflections in pitch plane. Flagged symbol indicates final jets-off test point.

SECRET

NATIONAL AERONAUTICS AND SPACE ADMINISTRATION

TECHNICAL MEMORANDUM SX-296

for the

U.S. Air Force

PERFORMANCE, STABILITY, AND CONTROL INVESTIGATION

AT MACH NUMBERS FROM 0.4 TO 0.9 OF A MODEL OF

THE "SWALLOW" WITH OUTER WING PANELS

SWEPT 25° WITH AND WITHOUT

POWER SIMULATION*

By Jack F. Runckel, James W. Schmeer,
and Marlowe D. Cassetti

ABSTRACT

Four outboard engines located above and below the wing provided propulsive thrust by means of hydrogen peroxide gas generators. Deflection of the engine nacelles, which incorporated swept lateral and vertical fins, in the vertical and lateral directions also produced control forces about the three body axes. Data were obtained at Mach numbers from 0.40 to 0.90 and at angles of attack and sideslip from 0° to 15°. The results indicate that the longitudinal controls were ineffective but that the directional and lateral controls were adequate. Jet interference effects on control characteristics were generally small.

INDEX HEADINGS

---

*Title, Confidential.